Study of Thermophysical Properties of the Slag to Predict the Slag Foaming Model: Effect of Cr_2O_3 Addition in EAF Slags.

by

Neha Meena

A Thesis Presented in Partial Fulfillment
of the Requirements for the Degree
Master of Science

Approved July 2023 by the
Graduate Supervisory Committee:

Sridhar Seetharaman, Chair
Terry Alford
Yuri Korobeinikov

ARIZONA STATE UNIVERSITY

August 2023

ABSTRACT

The characterization of interface properties in molten slag is crucial for understanding the interface phenomenon and the reactions between slag and metal. This study focuses on examining the influence of Cr_2O_3, an important surface active oxide, on the wettability and surface tension of slag. Industrial Electric Arc Furnace (EAF) slag with two different Cr_2O_3 contents (1 wt% and 3 wt%) was investigated using the sessile drop measurement technique at a high temperature of 1650°C. For the preparation of 3 wt% Cr_2O_3-doped slags, the following crucibles were used: Al_2O_3, Mo, and MgO. The behavior of crucibles, the dissolution process as well as its effect on the slag thermophysical properties were studied. For the evaluation of surface tension, Mo and MgO substrates were used. The contact angle was measured using the sessile drop method, and the surface tension was calculated using the Young-Laplace-based software. The interaction and wettability behavior between the slag and different substrates was studied. The effects of Cr_2O_3 content, in correlation with Al_2O_3, Mo, and MgO, as well as temperature, on the surface tension, and phase formation were analyzed using FactSage 8.2. The results indicate an increase in the formation of solid phases with Al_2O_3 and Mo dissolution into the slag. The composition of the MoO_3 is confirmed with the XRF and EDS analysis. Furthermore, an increase in the formation of the spinel phase was observed with the addition of chromium, which is confirmed via XRD. The increase in the CaCrMo-oxide-based spinel led to a decrease in the surface tension of the slag. The surface tension of the slag pre-melted in a Mo, decreases as the Cr_2O_3 content increases. The effects of the amounts of Cr_2O_3 in correlation with Al_2O_3, MgO, and MoO_3 on the slag foaming index were determined using the existing models in the literature.

ACKNOWLEDGMENTS

I would like to take this opportunity to express my sincerest gratitude to all those who have supported and guided me throughout my research and the completion of this thesis. First and foremost, I am immensely grateful to my supervisor, Prof. Sridhar Seetharaman, for his guidance, support, and feedback. His expertise and dedication have been instrumental in shaping this research and bringing it to fruition. I am truly fortunate to have had the opportunity to work under his mentorship.

I would also like to extend my heartfelt appreciation to Dr. Tetiana Shyrokykh and Dr. Yuri Korobeinikov for their insightful instructions and continuous assistance throughout my research journey. Their expertise and willingness to share their knowledge have significantly enriched my understanding of the subject matter. Without their guidance, this study would not have been possible. I would like to express my gratitude to my colleague Matthew Kurecki for his invaluable contributions.

I would like to acknowledge the Department of Energy (DOE) for providing funding for this research. Their financial support has not only allowed me to pursue this project but has also provided me with the resources necessary to learn and contribute to the success of this endeavor. I am grateful for the opportunity they have given me.

Furthermore, I would like to acknowledge the support of the Eyring Materials Center - ASU Core Facilities. The facilities and infrastructure such as the SEM/EDS, and XRD provided by the center have played a vital role in the successful execution of the experimental work. I am thankful to Mr. David Wright at ASU for his guidance, expertise, and support throughout the project.

My deepest appreciation and love goes to my parents. Without their love, support, and encouragement, I would not have been able to achieve my dream.

TABLE OF CONTENTS

LIST OF TABLES

LIST OF FIGURES

Chapter 1

INTRODUCTION

1.1 Motivation

Efficiency and cost reduction are currently at the forefront of EAF steelmaking. However, as we look ahead to the next 20 years, there is an increasing need for improved flexibility in selecting raw materials to enhance efficiency, minimize waste, and reduce the disposal of materials that could be repurposed for steelmaking operations. Additionally, there is a growing emphasis on improving the environmental performance of EAFs by reducing greenhouse gas emissions.

The primary objective of the proposed research is to develop an expert system that optimizes electric arc furnace (EAF) operations, diagnoses operational problems, and assists in making optimal raw material choices. By achieving these goals, the research aims to decrease the production of co-products, waste products, and hazardous wastes, while also improving energy efficiency.

There is a gap in the existing literature regarding the study of surface-active elements in slag, particularly the inclusion of Cr_2O_3. Although previous studies have investigated the effects of Cr_2O_3 in slag, limited research has specifically focused on its influence in EAF slag. The proposed thesis aims to address this gap by examining the effects of thermophysical properties, such as viscosity, density, and surface tension, as well as solid fraction, on the phenomenon of slag foaming. Additionally, the research aims to understand the structure and chemistry of Cr_2O_3 when combined with other oxides in the slag. By filling this gap and advancing our understanding of slag's physical properties and their performance, particularly in relation to slag

foaming, the research contributes to the broader objective of enhancing the efficiency, sustainability, and competitiveness of EAF steelmaking operations. Through its findings, the research will enable improved flexibility in raw material selection, decreased waste generation, and optimized energy consumption, ultimately leading to a more cost-effective and environmentally conscious EAF steelmaking process.

1.2 Background of Steelmaking

Steelmaking is the process of producing steel, a versatile and widely used metal alloy made primarily from iron and carbon containing less than 2% carbon and 1% manganese and small amounts of silicon, phosphorus, sulfur, and oxygen [1]. The steel industry is a vital component of modern society, with steel used in everything from buildings and bridges to automobiles and household appliances. Due to the continuous growth of the global population, there has been a corresponding increase in the demand for steel production, necessitating a consistent and ongoing expansion in the output of this essential industrial material. Today, there are several methods used in steelmaking, the Electric Arc Furnace (EAF) and the Basic Oxygen Furnace (BOF) are two common methods used in steelmaking. The critical difference between the routes is the type of raw materials they consume. For the BF-BOF route, these are predominantly iron ore, coal, and recycled steel, while the EAF route produces steel using mainly recycled steel and electricity, resulting in a lower carbon emission and less energy-intensive process [1]. While both have their advantages and disadvantages, there are several reasons why EAF should be used over BOF. The Electric Arc Furnace (EAF) is generally considered to be a more environmentally friendly option compared to the Basic Oxygen Furnace (BOF). The EAF process utilizes scrap steel and does not require the use of coal, which is a significant contributor to greenhouse gas emissions. Additionally, EAF is a more energy-efficient process compared to BOF

as it uses electricity instead of burning coal, hence EAF produces less air and water pollution than BOF. This makes EAF more suitable for locations with high electricity availability and lower coal availability. Based on the world steel report, the total crude steel production was 1,885.03 million tonnes in 2022 and 1,962.3 million tonnes in 2021. In 2022, the United States reported 85.8 million tonnes (Mt) of crude steel produced. As per the American Iron and Steel Institute (AISI), the United States has reported that it produces more than 70% of its crude steel through the Electric Arc Furnace (EAF) route. This places the United States in the fourth position in the world for steel production through EAF, behind China, India, and Japan as shown in figure 1.1.

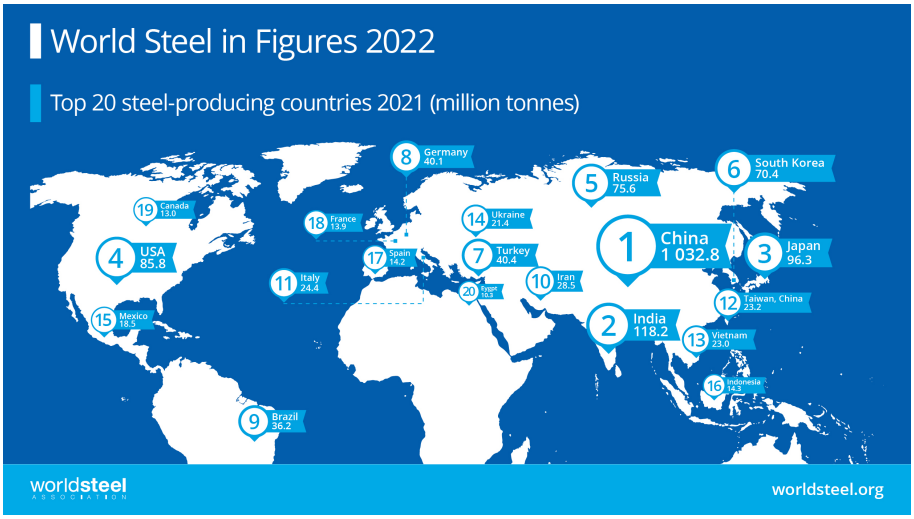

Figure 1.1: Top 20 Steel-producing Countries 2022 (Million Tonnes) [1]

Electric Arc Furnace [EAF]

EAFs have been used since the 1970s and consume high amounts of electric energy [3]. The primary objective of the EAF is to melt scrap steel and iron units into a generic liquid bath that can be refined and alloyed into any steel grade desired. Different types of scrap are fed to the electric arc furnace, as shown in figure 1.2.

The feed materials for EAF are mainly steel scrap and pig iron. However, steel scrap contains impurities such as phosphorus (P), aluminum (Al), manganese (Mn), and silicon (Si) that deteriorate the mechanical properties of steel products. When discussing the inputs and outputs of an EAF, we can consider the table 1.1, whereas it's important to note that the inputs and outputs of an EAF can vary depending on the specific operation, the type of steel being produced, and the environmental and regulatory considerations in place.

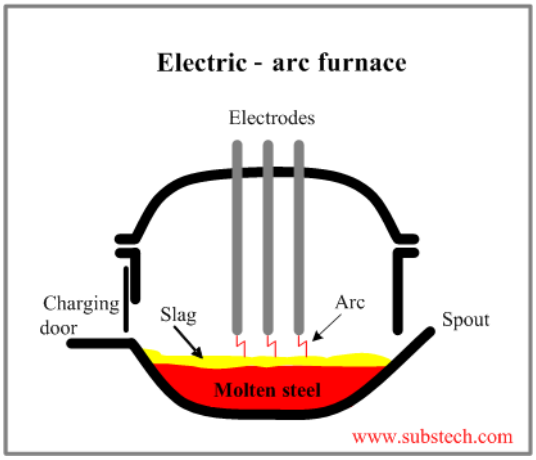

Figure 1.2: Simple EAF Block Diagram [21]

Input	Output
Scraps	Liquid Steel
Iron Units	Liquid Slag
Lime	Hot Off-gas
Dolomite Lime	Dust in hot off-gas
Electricity	Energy losses to water-cooled Components
Natural Gas	

Table 1.1: Input and Output of the EAF [3]

EAF operations involve several stages in the process of producing steel as shown in figure 1.3. The first stage is furnace charging, where scrap steel is loaded into the furnace. This is followed by the bore-in stage, where a cavity is created for the electrode and electric arc. In the melting stage, the intense heat generated by the electric arc melts the scrap steel, transforming it into a liquid state. The de-carbonization (De-C) stage involves injecting oxygen to remove carbon impurities from the liquid steel. In the de-siliconization (De-Si) stage, fluxes are added to react with silicon impurities, forming a floating slag layer. Further refining occurs in the de-manganese (De-Mn) and de-phosphorization (De-P) stages. The refining stage brings the steel to the desired temperature and chemical composition through the addition of alloys and refining agents. Final de-carbonization (De-C) and de-phosphorization (De-P) can be achieved by injecting additional oxygen. The tapping stage follows, where the liquid steel is discharged from the furnace and collected in a ladle, while the floating slag is also tapped separately. Subsequent processing and treatments are then carried out to produce the final steel product.

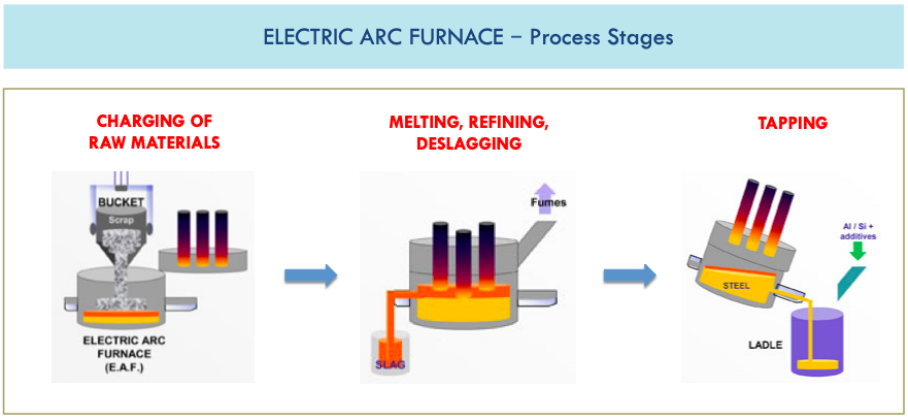

Figure 1.3: EAF Process Stage [15]

.

Chapter 2

LITERATURE REVIEW

2.1 Introduction to Slag

Slag is the by-product of the iron and steel industry, they are the ionic solution of oxides and fluorides and float on top of the liquid or partially liquid steel and can be removed using various techniques. Slag aggregates as shown in figure 2.1 are formed during the iron and steelmaking process as a result of the chemical reactions between the oxygen and other impurities present in the raw materials. Slag is a complex mixture of oxides and fluorides, such as calcium oxide, silicon dioxide, magnesium oxide, and aluminum oxide. It may also contain other elements such as sulfur, phosphorus, and carbon. In the electric arc furnace (EAF) steelmaking process, slag plays a crucial role in the production of steel. It acts as a refining agent, helping to remove impurities and adjust the chemical composition of the steel. The chemical composition and physical properties of the slag are carefully controlled during the steelmaking process to ensure the quality of the steel produced.

The primary functions of slag in steelmaking are as follows:

- Protect the steel from oxidation by forming a layer of slag on top of the molten steel, which prevents contact with atmospheric oxygen.
- Improve the quality of the steel by absorbing deoxidation products such as silicon dioxide (SiO_2) and aluminum oxide (Al_2O_3), which helps to remove impurities and inclusions from the steel.
- Protect the steel from nitrogen and hydrogen absorption, which can cause embrittlement, by reacting with these gases to form a slag.

- Insulate the steel to minimize heat loss by forming a layer of slag on top of the molten steel, which acts as a thermal barrier.
- Be fully compatible with the refractory lining to ensure efficient operation of the furnace and minimize wear and tear on the refractory materials.

Figure 2.1: EAF Slag Aggregates [23]

As the old maxim says "Take care of the slag and the steel will take care of themselves". Slag is typically analyzed for its chemical composition, including the levels of impurities such as heavy metals, as well as its physical properties, such as density and particle size distribution. The composition of EAF slag can vary widely depending on the raw materials used and the specific conditions of the process. Typically, EAF slag is composed of various oxides such as iron oxide (FeO) in the range of 10-40%, calcium oxide (CaO) in the range of 22-60%, silicon dioxide (SiO_2) in the range of 6-34%, aluminum oxide (Al_2O_3) in the range of 3-14%, magnesium oxide (MgO) in the range of 13-14% [16]. In addition, other minor components such as chromium oxide (Cr_2O_3), manganese oxide (MnO), titanium dioxide (TiO_2), and phosphorus pentoxide (P_2O_5) may also be present and can impact the phase relations of the slag. The calcium and silicon in EAF slag typically come from scrap.

In addition, ferroalloys that contain calcium and silicon, such as ferrosilicon and calcium silicide, may also be added to the EAF to help control the composition of the slag and ensure that the resulting steel meets the desired specifications. The source of aluminum in EAF slag is primarily the scrap metal that is used as a raw material in the steelmaking process. The primary source of magnesium in EAF slag is the dolomite refractory lining of the furnace. Dolomite is a type of limestone that contains magnesium carbonate ($MgCO_3$) in addition to calcium carbonate ($CaCO_3$). When the dolomite lining is exposed to the high temperatures and chemical reactions of the steelmaking process, it can react with the molten steel to form magnesium oxide (MgO), which then becomes part of the slag. The primary source of iron in EAF slag is the scrap metal that is used as a raw material in the steelmaking process. Other elements, such as chromium, titanium, and copper, are impurities that are present in the ferrous scrap.

2.2 Structure of Slags

Metallurgical slags are primarily composed of silicon dioxide (SiO_2), which forms the base structure of the slag. The building block for silicates is the Si-4O tetrahedron, consisting of a centrally placed Si^{4+} ion surrounded by $4O^-$ ions in a tetrahedral array figure 2.2 (a). These tetrahedra can join to other tetrahedra through the divalent O^{2-} ions sited at the corners of the tetrahedron, making it the fundamental building block for all silicates and aluminosilicates figure 2.2 (b). In pure SiO_2, each O^{2-} connects two Si^{4+} tetrahedra, resulting in a three-dimensional polymerized network structure. This polymerized structure makes SiO_2 referred to as a *"network former"*. However, when a basic oxide MO or M_2O, (where element M is K, Na, Li, Ca, Mg, Fe, Mn, Pb, Zn, Ni, or Cu) is added to SiO_2 based slag, the basic oxide dissociates into metallic cations and oxygen anions. The extra O^{2-} anions bond with silicon in

the SiO_2 structure and break up the network. The Ca^{+2} cations added in the form of CaO further decompose the network, making Ca^{+2} cations referred to as *"network breakers"* and basic oxides as *"network modifiers."*The thermophysical properties of silicate slags are highly dependent on the level of polymerization in the slag. Silicate slags contain both covalent and ionic bonds. When Al_2O_3 is introduced into the silicate network, Al^{3+} ions behave like Si^{4+} and exhibit fourfold coordination. Al_2O_3 acts principally as network formers, but when large amounts of Al_2O_3 are added, they also act as network breakers. Thus, Al_2O_3 is often referred to as an *"amphoteric."* Transition metal oxides such as FeO, MnO, ZnO, PbO, etc., do not form strong silicate molecules and break up the SiO_2 network structure less effectively. However, CrO is considered a basic oxide and reacts with acidic oxides present in the slag, helping to break down the slag structure and decrease its viscosity. On the other hand, the behavior of Cr_2O_3, which is also known as chromium oxide, is unclear in terms of its effect on slag viscosity. Unlike CrO, Cr_2O_3 has not considered a basic oxide and does not have a high pH. However, it can still interact with other oxides in the slag, and the specific nature of these interactions and their effect on viscosity is not yet fully understood.

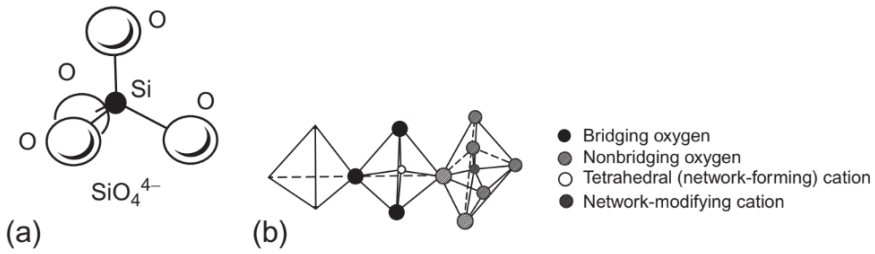

Figure 2.2: (a) Si^{4+} & $4O^{-}$ Bonds Arranged in the Form of a Tetrahedron, (b) Creation of a Network Through the Connection of Each O_2 to Two Si^{4+} Ions. [20].

There are multiple ways to describe or quantify the structures of silicate slags, and the following discussion will outline some of these parameters.

- **Basicity of slag** is expressed as the ratio of basic oxides to acidic oxides, which helps in representing the structure of slags. A slag with high basicity (more basic oxides than acidic oxides) will have a greater number of network breakers, resulting in a more depolymerized network and lower viscosity. On the other hand, a slag with low basicity (more acidic oxides than basic oxides) will have a lower number of network breakers and a more polymerized network, resulting in a higher viscosity. Several formulations have been used to express the basicity of slag. The most common approach is the use of a basicity index in which the basic oxides are placed on the numerator and the acid oxides on the denominator. Of these, by far the most commonly used is the V-ratio also commonly known as Binary Basicity (B_2) i.e.

$$\frac{\%CaO}{\%SiO_2} \tag{2.1}$$

- **NBO/T** is a ratio of Nonbridging Oxygen/Tetragonal Oxygen and **Q** are the two useful methods for representing the structure of EAF slags and can provide insight into the physical properties and behavior of these materials. NBO/T is a measure of the depolymerization of the melt and where T denotes the ions (Si^{4+}, Ti^{4+}, or Al^{3+}) in tetragonal configurations. It is the ratio of the mole fraction of available network-breaking oxides (where available indicates the total number of cations minus those on charge balancing duties) divided by the mole fraction of the network-forming oxides. A higher NBO/T value indicates a lower degree of polymerization. A lower degree of polymerization means that the slag is more fluid and easier to handle. Thus, (NBO/T) ratio is a kind of basicity index 2.2, that allows for corrections for cations acting on charge-balancing duties.

$$NBO/T = \frac{2(\Sigma XMO + \Sigma XM_2O - \Sigma XM_2O_3)}{(XSiO_2 + 2XAl_2O_3)} \tag{2.2}$$

where X is the mole fraction

XMO = XMgO + XCaO + XBaO + XFeO + XMnO +.....

$XM_2O = XLi_2O + XNa_2O + XK_2O$

It is easier to visualize polymerization than depolymerization, and thus prefer the parameter, Q; this is a measure of the polymerization of the melt and can be calculated from (NBO/T) using equation 2.3. A higher Q value indicates a higher degree of polymerization, meaning that the slag is more viscous and difficult to handle. For example, a slag with a Q of 3 means that each tetrahedron is connected to three other tetrahedra through bridging oxygens.

$$Q = 4 - \frac{NBO}{T} \tag{2.3}$$

- **Optical basicity** is called a fundamental indicator of slag basicity, and is a property that characterizes the basic nature of the slag composition. It is a measure of the ability of the slag to indicate its capacity to react with and absorb various impurities, such as sulfur, phosphorus, and silica, that may be present in the metal being processed. Using experimentally determined spectrographic information on a large number of glasses and Pauling's electronegativity data, the optical basicity for many components could be calculated. The table 2.1 shows the values of optical basicity (Λ) of slag components.

  The average optical basicity (Λ) for a slag of any composition can be calculated by means of the expression:

$$\Lambda = X_{\mathrm{Aox}}\Lambda_{\mathrm{AOx}} + X_{\mathrm{BOy}}\Lambda_{\mathrm{BOy}} + \ldots \tag{2.4}$$

  where,

Oxide	Optical Basicity (Λ)
Na_2O	1.15
CaO	1.0
MgO	0.78
CaF2	0.67
TiO_2	0.61
Al_2O_3	0.61
MnO	0.59
Cr_2O_3	0.55
FeO	0.51
Fe_2O_3	0.48
SiO_2	0.48

Table 2.1: Oxide Optical Basicity (Λ)

$$X = \frac{\text{mole fraction of component} \times \text{number of oxygen atoms in oxide molecule}}{\sum \text{mole fraction of component} \times \text{number of oxygens in oxide molecule of all components}}$$

While optical basicity is currently the best compositional parameter available that can be used to describe the composition (basicity) of a slag, it does not say anything about the physical properties of a slag. For example, consider the following "slag" composition:

% CaO = 62

% MgO = 8

% SiO_2 = 30

The optical basicity of this slag can be calculated as $\Lambda = 0.756$, which could be considered sufficiently basic to ensure good sulfur removal and minimum

refractory wear. However, the calculation of this number is meaningless because the slag listed above is completely solid at steelmaking temperatures, and it will only start to melt at 1790°C and will be fully molten at 1950°C. The application of the optical basicity concept to steelmaking slags is only useful if the slags are completely melted and it we have significantly more information, such as solidus and liquidus phase relations and viscosity data.

2.3 Effect of Chromium Oxides

Various studies have investigated the effect of Cr_2O_3 content on the viscosity of different types of slags. The findings reveal the following trends: Qiu [18] found that the viscosity of the blast furnace slag in the 29.3%CaO-26.7% SiO_2-8% MgO-22%TiO_2-14%Al_2O_3 system increased significantly as the Cr_2O_3 content increased from 0% to 4%. Xu [25] added 1%, 3%, and 5% Cr_2O_3 to the mold slag used for casting high-carbon chromium steel ($Cr_{12}MoV$). The results showed that with the increase of Cr_2O_3 content, both the melting temperature and viscosity increased. Li [13] studied CaO-SiO_2-MgO-Al_2O_3-Cr_2O_3 slag at 1550°C. In silicate networks, the Cr^{3+} ions act as the network formers and increase the degree of polymerization (DOP). The viscosity of the slag increases with the increase of Cr_2O_3. Xu [26] found that the viscosity of CaO-SiO_2-MgO-23.2% Al_2O_3-TiO_2 slag increased with the addition of Cr_2O_3, and the viscosity of the high Cr_2O_3-containing slag increased even more. Liu [14] reported the effect of the Cr_2O_3 content on the viscosity of stainless-steel-making slags. In low basicity (R = 0.57) slag, increasing the Cr_2O_3 content resulted in a lower viscosity. In slag with high basicity (R = 1.54), an increased Cr_2O_3 content resulted in increased viscosity. In 1964, J. H. Swisher and C. L. McCabe studied the addition of Cr_2O_3 significantly enhancing the foaming ability of the CaO-Si_2 slags. As the concentration of Cr_2O_3 increased, the viscosity of the slags decreased,

promoting the formation of gas bubbles and foam stability. The surface tension of the slags also decreased with Cr_2O_3 addition, further facilitating the foaming process. Additionally, the study examined the role of Cr_2O_3 in modifying the slag structure. It was found that Cr_2O_3 incorporation led to changes in the chemical composition and crystalline phases of the slags, which influenced their foaming behavior. The study on the interfacial properties of the Cr_2O_3 bearing slag is limited.

The presence of surface active oxides, such as B_2O_3, Cr_2O_3, Fe_2O_3, Na_2O, and P_2O_5, in EAF (Electric Arc Furnace) slag can significantly impact its properties. Understanding the sources and effects of Cr_2O_3 in EAF slag is particularly important. Several sources contribute to the presence of Cr_2O_3 in the slag. Firstly, chromium-containing alloys or materials in the scrap metal can oxidize during melting, leading to the formation of Cr_2O_3 in the slag. Additionally, the addition of ferrochrome alloy promotes chromium oxidation, resulting in the incorporation of Cr_2O_3 into the slag. Erosion of chrome-based refractories used in the furnace can also release chromium, further contributing to Cr_2O_3 formation. Moreover, previous slag carryover can introduce Cr_2O_3 into the current slag composition. However, the existing literature lacks sufficient data on the ideal Cr_2O_3 content in EAF slag, highlighting the need for further research in this area. Systematic investigation can provide valuable insights into optimizing slag composition and properties in EAF operations.

2.4 Slag Foaming

In an EAF, scrap steel is melted by an electric arc generated between electrodes and the charge materials in the furnace. During the melting process, a layer of slag forms on top of the molten steel as shown in figure 2.3. Electric arc furnaces (EAFs) use the method of slag foaming to increase the productivity and efficiency of the steelmaking process. One of the most significant advantages of slag foaming

is its ability to increase the heat retention of the furnace. The foam layer traps heat inside the furnace, reducing heat losses through the walls of the furnace. This results in a reduction of energy costs and an improvement in the efficiency of the steelmaking process. Additionally, the foam layer promotes better mixing of the slag and steel, improving the transfer of heat from the electrodes to the steel, and resulting in a reduction in sound, vibration, and electrode consumption during the melting process. It has been studied to decrease both energy consumption (around 10–30%) and refractory consumption (around 25–63%)[7].

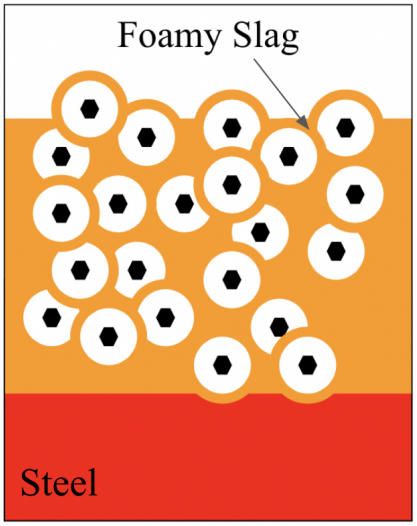

Figure 2.3: Schematic of EAF Slag Foaming

There are basically two requirements for foaming:

- Reactions or processes that generate small gas bubbles
- Suitable slag properties to keep the bubbles as stable foam

The driving force for slag foaming is pneumatic energy provided by CO generation during melting-refining in EAF. During the slag foaming process, carbon is injected into the slag and reacts with FeO in the slag-producing CO, which is mainly responsible for the foaming effect as in reaction 2.5. CO(g) formation is also related to the

reaction between C (from the metal) and oxygen, as shown by reaction 2.5 & 2.6.

$$\mathrm{C(Injected)} + \mathrm{FeO} \longrightarrow \mathrm{Fe} + \mathrm{CO} \tag{2.5}$$

$$\mathrm{C(in\,metal)} + (1.5)\,\mathrm{O_2} \longrightarrow \mathrm{CO} \tag{2.6}$$

Reaction 2.5 occur at the interface between carbon and slag (c-s), while equations 2.6 take place at the interface between the gas and metal (g-m). Equations 2.5 and 2.6 represent chemical reactions that are responsible for the formation of CO(g) and play a critical role in the mass transfer among the metal, slag, carbon, and gas phases. These reactions are considered to be a necessary condition for slag foaming. The generated gas is responsible for the bubbles and foam formation, which should remain at the upper liquid surface, even after the reaction between FeO and C is completed. Foaming of slag should not be mistaken for the simple formation of gas bubbles in a liquid. In the case of gas bubbles, they are dispersed throughout the entire liquid and the expansion of the slag is due to the gas bubbles. The expansion is temporary and goes away quickly after the gas is no longer being generated. On the other hand, true slag foaming is different. It creates a stable foam layer that can last for several minutes even after the gas generation stops. This foam layer is created by injecting gas into the slag, and it provides several benefits such as better heat transfer and improved chemical reactions. So, it's important to understand the difference between gas bubbles and true slag foaming to optimize the steelmaking process. The foam can have relatively small foam bubbles like foam on beer or larger bubbles like soap bubble foam on water. In general, the small bubbles result from chemical reactions and the resulting foam is fairly stable. In general, gas injection produces larger bubbles and less stable foam. To keep bubbles in the slag stable and maintain a foam, it is important to have suitable slag properties.

The following are some of the properties that can help maintain stable slag foam:

- Basicity - Achieving a balance between refractory and fluxing oxides is key for EAF slag engineering. Refractory oxides increase viscosity, fluxing oxides increase fluidity, but excess negatively affects foam. Basic slag compositions, which have a higher concentration of basic oxides than acidic oxides, are generally better for foam stability. The basic oxides react with acidic gases such as CO_2 and SO_2 to form solid particles, which help to stabilize the bubbles.
- Temperature - If the temperature is too low, the slag may solidify and prevent bubble formation. Also, if the temperature is too high, the slag may become too fluid, causing the bubbles to rise quickly to the surface and burst.
- FeO concentration - Iron oxide, particularly FeO, is a major component of slag and can have significant effects on the properties of the slag. Low FeO content in the slag, less than 10 mass-%, can result in a viscous slag that is difficult to foam. On the other hand, if the FeO content is too high, greater than 40 mass%, the slag becomes too fluid, and the gas bubbles cannot remain in the liquid. This can lead to a reduction in foam stability.
- Surface tension - Low surface tension helps to stabilize the bubbles and prevent coalescence (merging of bubbles). This can be achieved by using slag with a high concentration of basic oxides such as CaO and MgO.
- Viscosity - Optimal range of viscosity, allows the bubbles to be stable. If the slag viscosity is too low, the bubbles will quickly rise to the surface and burst. On the other hand, if the viscosity is too high, the bubbles will not be able to rise and will be trapped in the slag.
- Suspended second-phase particles - The solid particles in the slag act as gas nucleation sites, leading to a high amount of small gas bubbles in the slag. Additionally, the suspended particles can change the effective slag viscosity.

2.5 Thermophysical properties

Viscosity

Viscosity (μ) is a physical property of a material that describes its resistance to flow and is an essential factor in managing slag flow behavior and minimizing refractory wear. It is a measure of the ability of a fluid to sustain shear stresses and plays a crucial role in many high-temperature phenomena that are important for advancing process control and product quality in molten-metal processing and casting. The viscosity of molten metals and slags is influenced by various factors such as temperature, composition, atmosphere, shear rate, and thermal history. While most metallic melts and molten slags exhibit Newtonian fluid behavior with viscosities independent of shear rate, there are conflicting requirements when it comes to slag performance. In metallurgical practice, an ideal slag should have high fluidity (low viscosity) to facilitate efficient flow. On the other hand, for refractory wear considerations, a good slag should possess low fluidity (high viscosity) to minimize penetration, and reaction, and ensure the formation of a protective coating. Finding the optimum viscosity range for slag is crucial. If the viscosity is too low, bubbles pass through the slag quickly, resulting in shallow foam. Conversely, excessively high viscosity leads to localized reactions and the bursting of bubbles like geysers, resulting in poor foaming [24] as shown in figure 2.4. Therefore, a balanced and carefully controlled viscosity is essential to achieve effective slag foaming in electric arc furnaces, balancing the requirements of fluidity for efficient flow and viscosity for refractory protection.

Surface Tension and Density

Surface tension is a fundamental property that manifests in all surface and interfacial phenomena. It affects droplet size and coalescence behavior, which is crucial

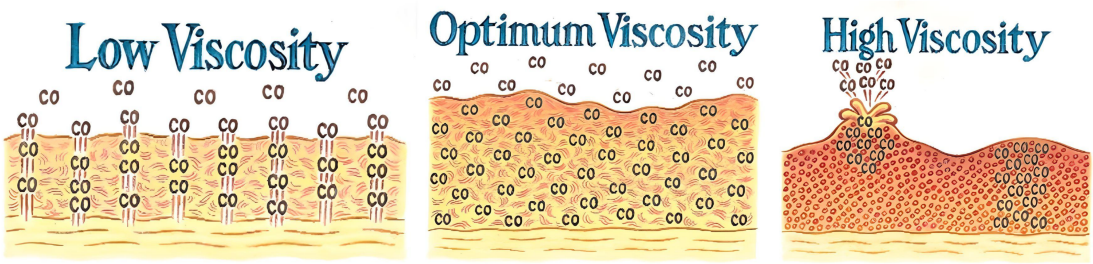

Figure 2.4: Schematic of Viscosity Effect on Foaming [24].

in heavily stirred reactors in process metallurgy for controlling reaction rates. The surface tension is affected by surface-active components, which may impose significant surface tension gradients that give rise to the Marangoni effects. The surface tension of slags and steel or the interfacial tension plays a dominant role in iron and steelmaking processes. Surface tension is also sensitive to the structure of liquid slags. According to Lee and Zhang [12], the motion of the slag caused by surface tension phenomena (wettability) between the refractory and slag essentially caused the local corrosion of refractories at the slag surface. This is due to the slag film motion which accelerates the dissolution rate of the refractory and also induces the abrasion of some refractories as shown in figure 2.5. The active film motion is dominantly induced by the Marangoni effect and/or change in the form of the slag film due to the variation of the surface tension and the density of the slag. For practical applications, surface tension is necessary to understand the wettability and infiltration behavior of molten slag/metal into refractories, metal separation, and slag foaming. Most common laboratory test is depicted in figure 2.6 to observe the interaction and wetting behaviour of the slag with the substrate/refractory material.

The interfacial tension between solid and liquid can be calculated by *Young's equation* as follow:

$$\sigma_{SL} = \sigma_{SG} - \sigma_{LG}\cos(\theta) \tag{2.7}$$

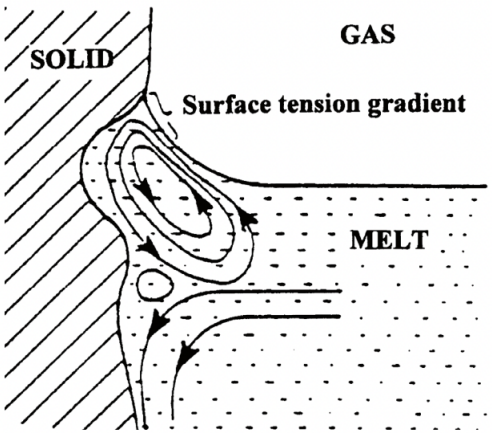

Figure 2.5: Illustration of the Motion of the Slag Film Caused by the Surface Tension Phenomena Between the Refractory and Slag [12].

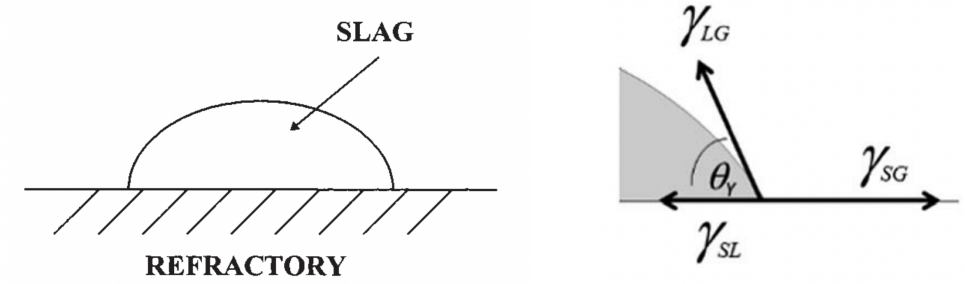

(a) a (b) b

Figure 2.6: (a) Slag/Refractory Laboratory Test [12], (b) Young's Equation Represents the Balance of Forces in the Contact Line of the Solid, Liquid, and Gaseous Phase [2].

where:

σ_{SL} - represents the interfacial tension between the solid phase and the liquid phase

σ_{SG} - represents the surface energy of the solid phase

σ_{LG} - represents the surface tension of molten slag, and

θ - represents the contact angle between the solid phase and the liquid phase.

Wetting replaces an area of the gas-solid interface by an equivalent area of a solid–liquid interface. This effect is usually accompanied by changes in the area of the liquid–gas interface. These surface relationships vary with the system's conditions and can change during the wetting process depending on the topography. Since each interface has its own specific surface energy, the result is a net increase or decrease of the total interfacial energy [2].

Suspended second-phase particles

Previous research has shown that foaming characteristics improve with decreasing surface tension and increasing the viscosity of the slag. However, it was also shown that the presence of suspended second-phase particles in the slag had a much greater impact on foaming than surface tension and slag viscosity. In layman's terms, the slags that achieve the best foaming properties have a consistency (fluidity) that falls between "creamy" and "fluffy", with "watery" and "crusty" on the extreme ends of the spectrum. This means that these "optimum" slags are not completely liquid ("watery") but are saturated with respect to CaO (Ca_2SiO_4) and/or MgO (Magnesia - wustite solid solution). These second-phase particles serve as gas nucleation sites, which lead to a high amount of favorable small gas bubbles in the foaming slag. The term effective viscosity was defined to relate the number of second-phase particles in the slag and viscosity as follows:

$$\eta_e = \eta \left(1 - 1.35\Theta\right)^{-\frac{5}{2}} \tag{2.8}$$

where:

η_e - effective viscosity of the slag

η - viscosity of the molten slag

Θ - a fraction of precipitated solid phases

The equation 2.8 is also known as the *Einstein-Roscoe equation* which describes the effect of the amount of solid particles and their size distributions on their effective viscosity values.

2.6 Slag Foaming Index

As mentioned in section 3.1, slag foaming refers to the presence of gas bubbles in molten slag, either introduced intentionally or formed through chemical reactions. This causes an increase in the volume of the slag and affects its height. Foaming is beneficial because it creates a protective layer, which helps prevent material and temperature losses and enhances refining processes. However, uncontrolled or excessive slag foaming can result in slopping, where the slag overflows from the furnace. This poses safety risks to personnel and can damage equipment [5]. Overall, calculating and controlling slag foaming in EAFs is essential for optimizing the steelmaking process, ensuring safety, improving energy efficiency, and minimizing environmental impacts.

The importance of understanding the foaming behavior of slag was realized by metallurgists quite early. As early as 1959, Cooper and Kitcher [4] measured the time required to decay a given volume of foam or foam life for CaO-SiO_2 slag. They found that a decrease in temperature and basicity increased the foam life but a small addition of P_2O_5 significantly increased it. Swisher and McCabe [22] reported that the addition of Cr_2O_3 in CaO-SiO_2 slag increased foam life. Hara et al. [6] found that the foam life, foam height, and surface tension of slags are related to CaO-FeO, SiO_2 -FeO, and CaO-SiO_2 -FeO systems. Fruehan and his associates [7, 9, 19, 27, 10] systematically measured and correlated the foaming characteristics for different slags of importance to iron and steelmaking. To quantify the foaming characteristics, they

measured the foaming index defined as [8]:

$$\Sigma = \frac{h}{U_s} \tag{2.9}$$

where h is the height of the foam at a steady state when the gas with superficial velocity U_s is passed through it.

Several researchers have proposed different models to define the foaming index by incorporating the physical properties of the slag. These models aim to establish a relationship between the measured foaming index and the calculated physical properties of the slag. The physical properties most frequently mentioned in these studies are the slag's viscosity (μ), surface tension (σ), and density (ρ). By considering these properties, researchers have gained valuable insights into the foaming behavior of slag in various metallurgical processes. These studies have contributed to the development of improved strategies for controlling and optimizing slag foaming.

Several models have been proposed by researchers to define the foaming index using the physical properties of the slag. The relationships between the foaming index and the physical properties of slags. The physical properties most frequently mentioned in these studies are the slag's viscosity (μ), surface tension (σ), and density (ρ). By considering these properties, (equation 2.10) is developed by Kim–Min–Park [11], where C is the constant that depends on the type of the slag.

$$\Sigma = C\left(\frac{\mu}{\sqrt{\rho\sigma}}\right) \tag{2.10}$$

Foamy slag depends on the rise of bubbles formed by the described reactions 2.5 2.6, it was found that slag viscosity is extremely important to effective foaming. The increase in viscosity decreases the drainage rate of the liquid foam, giving the bubble a longer residence time, and increasing foam height and stability. Figure 2.4 shows the effect that the viscosity has on the foaming index. An optimal slag is not completely liquid, whereas the presence of solid particles is crucial. The solid particles

act as nucleation sites for the bubbles, causing a large amount of small bubbles to be generated in the foamy slag. Figure 2.7 shows that an increase in viscosity provides an increase in the foaming index, reaching a peak where the optimal slag is found. However, an excessive increase in viscosity forms crusty slag, and the presence of solid particles begins to be harmful, because bubble ascension is impaired. Unfortunately, slag foaming is a highly dynamic process that is difficult to control. Optimizing surface tension, density, and viscosity is essential for achieving optimal slag foaming performance. Lowering surface tension promotes foam stability and smaller bubble sizes while adjusting density influences buoyancy and foam structure stability. Controlling viscosity affects liquid drainage and bubble coalescence. By adjusting slag composition, incorporating additives, and employing thermal treatments, these parameters can be optimized to strike a balance between foam stability, bubble size distribution, and gas retention. The resulting improvements enhance the efficiency of slag foaming processes, benefiting applications such as metallurgical operations and waste treatment.

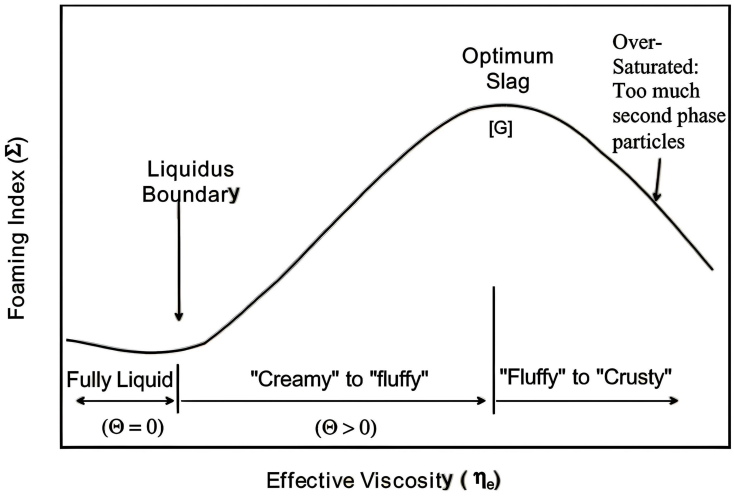

Figure 2.7: The Relationship Between the Foaming Index and Effective Viscosity.[17]

Chapter 3

EXPERIMENTAL SETUP

3.1 Sample preparation

The experimental investigation employed a specific approach aimed at equilibrating industrial slag samples at a temperature of 1600°C, conducting pre-melting procedures under the Ar-atmosphere, and analyzing the impact of varying Cr_2O_3 contents on the slag's phases, phase compositions, and phase fractions. The sample preparation process involves two main steps: (1) Preparing the industrial slag of composition S1 (as shown in Table 3.1) and subsequently doping Cr_2O_3 in the slag to achieve the desired S2 composition 3.1, (2) pre-melting the slag: it helps to achieve a more uniform composition, facilitates desired chemical reactions, removes volatile impurities, and improves processability. These benefits contribute to better control over the properties and behavior of the slag, making it more suitable for experimental investigations.

In the first step, the industrial slag is collected and then crushed into small particles using a grinding mill facility at a Commercial Metal Company (CMC) in Mesa. It is important to ensure that the particles are of uniform size and free from any impurities. The X-ray fluorescence spectroscopy (XRF) analysis has been performed on the industrial obtained slag i.e. S1 composition shown in table 3.1. Once the S1 slag is analyzed, the second step involves doping Cr_2O_3 into the slag. In this process, a measured amount of the S1 slag is taken and placed in a crucible, then Cr_2O_3 which is the doping material, is then added to the S1 slag. The amount of Cr_2O_3 added will depend on the desired doping concentration i.e. 3 wt% (S2) slag in table 3.1.

Sample	CaO	SiO_2	MgO	P_2O_5	SO_3	TiO_2	Cr_2O_3	Al_2O_3	MnO	FeO	Total
S1	32.47	13.69	9.57	0.80	0.32	0.60	1.07	6.10	5.90	29.48	100.00
S2	31.84	13.42	9.38	0.78	0.31	0.59	3.00	5.98	5.78	28.90	100.00

Table 3.1: Composition of Slag S1 and S2

This utilization of industrial slag offered the advantage of enabling the independent manipulation of Cr_2O_3 contents in a controlled manner. Given that both Cr_2O_3 and FeO can exist in various oxidation states, it was crucial to regulate the system's oxygen potential to obtain results representative of real industrial conditions. Thus, the experimental approach sought to establish the desired oxygen potential by employing an argon (Ar) atmosphere during the pre-melting phase of the slag composition. The choice of the crucible is also a very crucial step while performing the pre-melting of the slag. The crucible can dissolve into the slag and can change the composition of the slag significantly. It can affect the crucible when using high FeO-containing slag in the pre-melting of EAF slag in a laboratory. The corrosive nature of FeO can cause erosion and dissolution of the crucible material, leading to wear and degradation. Crucible selection becomes crucial, with materials like graphite or refractory ceramics being more resistant to FeO corrosion. Contamination is another concern, as FeO-rich slag can transfer its constituents to subsequent experiments or samples.

After careful consideration, three crucibles were used for pre-melting to understand the behavior and infiltration of the crucible to the slag as follows:

- **Alumina (Al_2O_3) Crucible**

  High-purity Al_2O_3 ceramic material is renowned for its exceptional resistance to high temperatures, withstanding up to 1700°C, and its ability to resist chemical

corrosion. It is widely utilized in high-temperature applications, particularly in the melting and handling of diverse metals and compounds. Al_2O_3 crucibles are meticulously chosen based on their compatibility with the slag composition, capacity to endure elevated temperatures and suitability for the furnace dimensions. The EAF slag samples, in the form of pellets, are loaded into the Al_2O_3 crucibles. The loaded crucibles are placed within a High-Temperature Tube-furnace, and the temperature is gradually increased to initiate the pre-melting process under an Argon atmosphere. The specific temperature and heating rate are determined based on the slag composition and desired outcomes. To obtain the maximum liquid phase, the furnace is heated to 1650°C. Once the pre-melting process concludes, the crucibles are carefully extracted from the furnace after it cools down. The cooled slag is then primed for subsequent analysis. Observation revealed that the crucible experienced expansion within the furnace tube due to thermal expansion (see figure 3.1 (a)). Consequently, it became challenging to remove the crucible from the furnace. Figure 3.1 (b) shows that the slag infiltrated into the crucible. The removal of slag from the Al_2O_3 crucible is a critical step, which leads to the fracture of the crucible, resulting in the retrieval of pre-melted slag in fragments as shown in figure 3.1(c). These fragments are subsequently crushed and ground using a grinding mill to obtain finely powdered slag for further analysis. The composition of the pre-melted slag in the Al_2O_3 crucible is presented in table 3.2. From the XRF analysis, it has become clear that a substantial degree of mixing occurred between the crucible material and the EAF slag during the pre-melting process. The initial composition of the S1 slag, containing approximately 6 wt% Al_2O_3, has experienced a notable increase to approximately 31 wt% in the resulting pre-melted slag. This significant rise in the Al_2O_3 content demonstrates the extent of in-

teraction and incorporation of the crucible material into the molten slag during the pre-melting process. Such outcomes suggest that further investigation and optimization of the pre-melting process parameters and crucible selection may be required to mitigate the unintended mixing and ensure the integrity and purity of the pre-melted slag composition. The typical EAF slag contains 3-14% of Al_2O_3. Studying the 30% Al_2O_3 content in the EAF slag is not the focus of this study, but it would be interesting to understand the extent of heavy cross-mixing between the Al_2O_3 substrate and the slag.

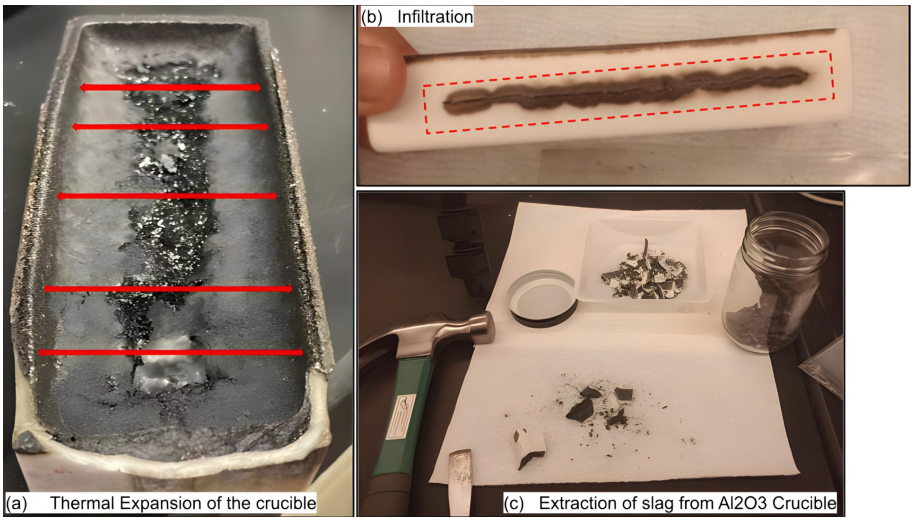

Figure 3.1: Behaviour of the Al_2O_3 Crucible During Pre-melting of the Slag

Sample	**Al_2O_3**	**CaO**	**Cr_2O_3**	**FeO**	**MgO**	**MnO**	**P_2O_5**	**SiO_2**	**SO_3**	**TiO_2**	**Total**
S1-Al_2O_3	34.57	22.19	0.86	20.89	5.99	4.09	0.60	10.33	0.18	0.30	100.00
S2-Al_2O_3	35.25	20.94	2.96	20.41	5.59	4.09	0.56	9.65	0.22	0.33	100.00

Table 3.2: Composition of Samples S1-Al2O3 and S2-Al2O3

- **Molybdenum (Mo) Crucible**

  The choice of using the Mo crucible based primarily due to the high melt-

ing point, oxide formation, and thermal stability of molybdenum. The high melting point of molybdenum ensures that the crucible remains solid during the pre-melting process, preventing the slag from melting into or adhering to the crucible. Additionally, molybdenum forms a protective oxide layer (MoO_3) when exposed to air or high temperatures, acting as a barrier that prevents direct contact between the slag and the crucible. This oxide layer inhibits slag adhesion to the crucible. Collectively, these characteristics make molybdenum crucibles highly effective in preventing slag from sticking during the pre-melting process. The process of pre-melting using the Mo crucible is identical to that of the Al_2O_3 crucible. Figure 3.2 (a) depicts the initial pellets being placed in the Mo crucible before pre-melting. It was interesting to observe the crucible's appearance afterward, as it was evident that the slag had splashed onto the rim (as shown in figure 3.2 (b) and (c)) during the pre-melting process, suggesting foaming at high temperatures. The extraction of the slag from the crucible is easy in this case since the slag does not adhere to the surface, unlike the Al_2O_3 crucible. The slag is collected to grind using a ball milling, for further analysis. The composition of the pre-melted slag in the Mo crucible is presented in table 3.3 analyzed via XRF analysis. To confirm the composition of Mo, the mass loss study and EDS analysis have been performed which is discussed in section 4.2. Additionally, these crucibles are polished and cleaned for reuse in subsequent pre-melting of the slag. One crucible is being used for up to four runs of pre-melting of the slag, after the fourth attempt there is a visible difference in the shape of the Mo crucible, and a heavy corrosive effect is observed shown in figure 4.9.

- **Magnesia Oxide (MgO) Crucible**

  Due to the significant dissolution of Al_2O_3 and Mo observed during the pre-

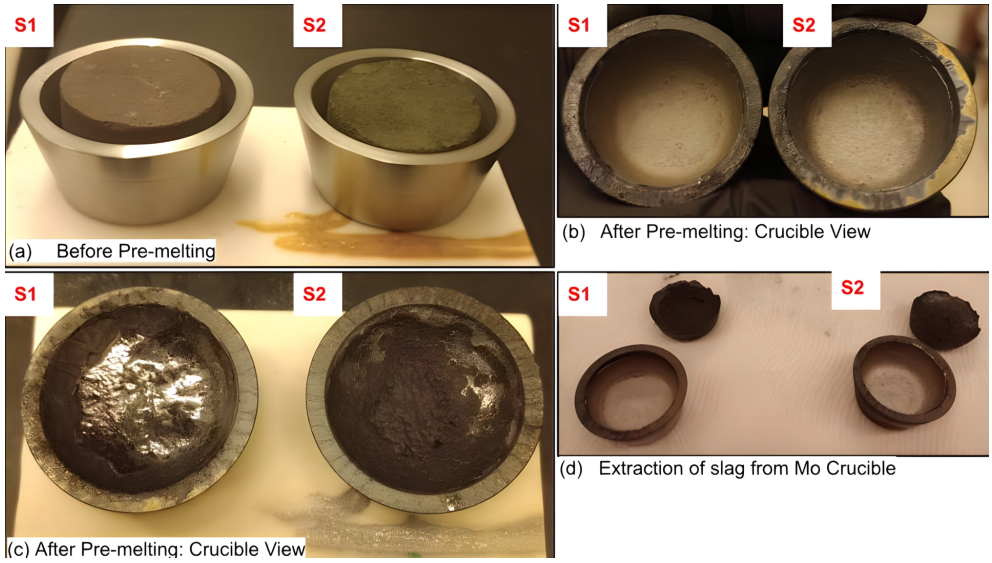

Figure 3.2: Behaviour of the Mo Crucible During Pre-melting of the Slag

Sample	**Al_2O_3**	**CaO**	**Cr_2O_3**	**FeO**	**MgO**	**MnO**	**MoO_3**	**P_2O_5**	**SiO_2**	**SO_3**	**TiO_2**	**Total**
S1-Mo	6.50	30.32	1.00	18.93	5.92	5.25	19.09	0.24	12.25	0.00	0.49	100.00
S2-Mo	6.58	29.12	3.39	19.31	6.05	5.18	17.27	0.26	12.36	0.00	0.47	100.00

Table 3.3: Composition of Samples S1-Mo and S2-Mo

melting process, the utilization of MgO (magnesium oxide) crucibles has become essential. These crucibles are specifically chosen for their ability to withstand the extreme temperatures involved in pre-melting, ensuring a reliable container for the process. The remarkable thermal conductivity of MgO crucibles promotes efficient heat transfer, resulting in faster and more uniform heating of the slag. Furthermore, MgO crucibles possess excellent thermal shock resistance, enabling them to endure rapid temperature fluctuations without developing cracks or experiencing failure. While other refractory materials may be suitable alternatives, MgO crucibles offer a unique combination of properties that make them particularly well-suited for the pre-melting of EAF slag. It is

worth noting that the existing saturation of industrial slag with MgO further enhances the suitability of MgO crucibles for this purpose. Figure 3.3 illustrates the behavior of slag inside MgO crucibles after reaching a temperature of 1650°C. Unlike Al_2O_3 and Mo crucibles, the MgO crucibles remain intact without any cracks or infiltration. The absence of cracking or infiltration ensures the integrity of the crucible, preventing any unwanted reactions or impurities from compromising the molten slag. This further reinforces the advantage of MgO crucibles over alternatives such as Al_2O_3 and Mo, making them an ideal choice for the pre-melting of EAF slag.

Figure 3.3: Behaviour of the MgO Crucible During Pre-melting of the Slag

3.2 Sessile Drop Experiment

A sessile drop experiment is commonly used to measure the contact angle and wetting behavior of a liquid on a solid substrate. In the case of studying high-temperature Electric Arc Furnace (EAF) slag, a sessile drop experiment can provide insights into the interaction between the molten slag and the substrate at elevated temperatures.

The Molybdenum substrate used in this study has dimensions of 1.00" in diameter and 0.125" in thickness. It possesses a purity greater than 99%. Two types of MgO substrates were also employed, namely a 26 mm diameter MgO Block and a MgO Single Crystal substrate measuring 1.00" in diameter and 0.5mm in thickness. All the substrates are obtained from MSEsupplies. To minimize the influence of substrate surface roughness on the experiments, the substrates were meticulously sanded and polished with sandpaper prior to each wetting experiment. The wetting behavior was characterized using the measurement of contact angle, a common method for assessing wettability. The contact angle between the molten slag and the substrate was observed using images captured by a CCD camera in conjunction with specific software.

The wetting behavior was observed using a High-Temperature horizontal tubular furnace, as illustrated in figure 3.5. The powdered slag samples were accurately weighed and then compacted into cylindrical molds under a specific pressure using a pellet press. These cylindrical samples were placed on the substrate, which was positioned on an alumina plate base to safeguard the furnace tube against any potential slag spillage. Prior to heating, the furnace was purged with high-purity argon gas (99.99% purity) and maintained throughout the entire process to prevent slag oxidation. All experiments were carried out under a controlled atmosphere of high-purity argon to avoid FeO oxidation. The slag was heated to the designated temperature of 1650°C and held for 10 minutes. The changes in droplet profile were continuously recorded by a high-resolution camera to monitor the alterations in contact angle. To ensure accuracy, photographs were captured and measured three times to calculate the average contact angle. Furthermore, each experiment has been repeated a minimum of two times to enhance the reliability of the results.

In the present work, surface tension is calculated using "Tropfenberechnung Po"

which is based on the Laplace equation. The Young-Laplace equation is used to calculate the surface tension of molten slag. The Young-Laplace equation describes the relationship between the pressure difference across the interface of a curved liquid droplet and the surface tension of the liquid. The equation 3.1 gives the pressure difference (ΔP) across the liquid surface at any point in terms of the surface tension (γ) and the two principal radii of curvatures at that point. The Young-Laplace equation is given by:

$$\Delta P = \gamma \left(\frac{1}{R_1} + \frac{1}{R_2} \right) \tag{3.1}$$

where ΔP is the pressure difference across the liquid interface, γ is the surface tension, R_1 and R_2 are the principal radii of curvature at that point.

In sessile drop by symmetry, the two principal radii of a surface element at the apex of the drop are equal. The internal pressure at the apex is given by Equation 3.2:

$$\Delta P_o = (\frac{2\gamma}{R_o}) \tag{3.2}$$

where R_o is the radius of curvature of the drop at the apex and pressure P_o just below the apex is a minimum.

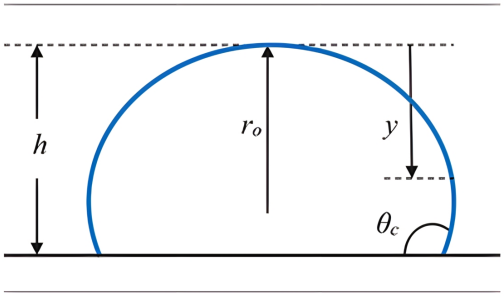

Figure 3.4: Young-Laplace Equation in Sessile Drop

The pressure at any point y below the apex is given by equation 3.3:

$$P(y) = P_0 + \rho g y = \frac{2\gamma}{\rho} + \rho g y \tag{3.3}$$

where $P(y)$ is the pressure at a point y below the apex, P_0 is the pressure at the apex, ρ is the density of the fluid, g is the acceleration due to gravity, and γ is the surface tension.

The pressure at other points inside the drop increases linearly with depth below the apex The pressure at the base of the drop is a maximum given by p(h) = p0+gh.

The mean curvature equation 3.4 of a surface element below the apex can be calculated using the Young-Laplace equation 3.1 and 3.3 :

$$c = \frac{1}{R_1} + \frac{1}{R_2} = \frac{2}{r_0} + \frac{pgy}{\gamma} \tag{3.4}$$

where c represents the mean curvature, R_1 and R_2 are the principal radii of curvature, ρ is the density of the fluid, p is the pressure at that point, g is the acceleration due to gravity, and γ is the surface tension.

When a liquid droplet is placed on a solid surface, it undergoes interfacial tension phenomena resulting in the formation of a curved interface. This curved interface exhibits varying curvature, which can be precisely quantified in terms of the mean curvature of the droplet interface. The interfacial tension plays a fundamental role in the determination of the Laplace pressure difference, as it is one of the crucial parameters influencing the curvature of the droplet interface. Mathematically, the Laplace pressure difference across the curved interface of the droplet is related to the surface tension of the liquid and the contact angle between the droplet and the solid surface. The interfacial tension serves as an essential factor in determining the Laplace pressure difference, which serves as a measure of the curvature of the droplet interface. In the derivation of the Young-Laplace equation for a sessile drop,

the interfacial tension existing between the liquid and the solid surface is implicitly encompassed within the contact angle term. The contact angle represents the angle formed between the tangent to the droplet at the point of contact with the solid surface and the solid surface itself. The determination of the contact angle arises from the equilibrium of forces acting at the three-phase contact line, where the liquid, solid, and gas phases meet. Among these forces, interfacial tension contributes to the contact angle, along with the adhesive forces between the liquid and solid and the cohesive forces within the liquid. The surface tension of the liquid, which is intrinsically linked to the interfacial tension, governs the magnitude of the Laplace pressure difference. Simultaneously, the curvature of the droplet interface is determined by the shape of the droplet itself and the contact angle it forms with the solid surface.

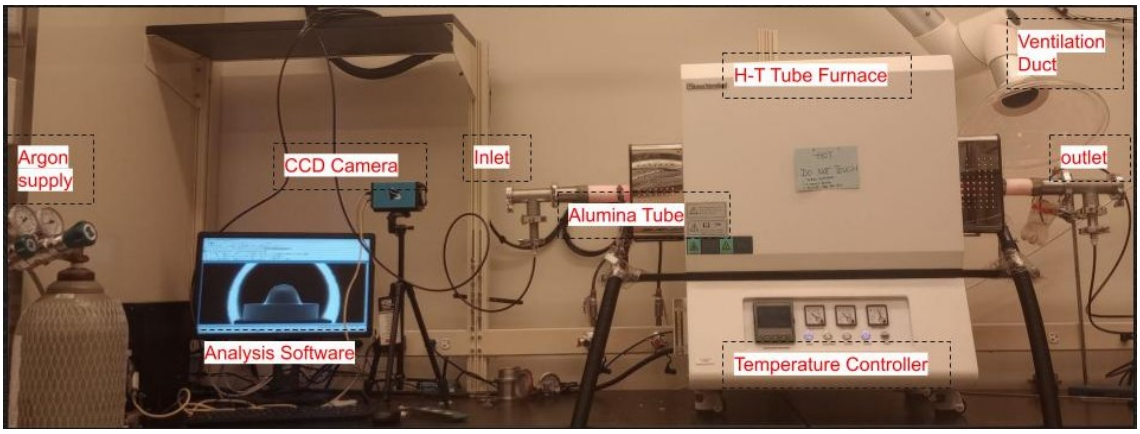

Figure 3.5: Sessile Drop Experimental setup

3.3 Sample Analysis

The slag used in this study was received from the steelmaking industry. Upon obtaining the slag, the chemical compositions were carefully inspected using the XRF technique. To perform XRF analysis, the sample is prepared and placed in an XRF instrument. The instrument emits high-energy X-ray photons that interact with the

atoms in the sample, causing inner shell electrons to be ejected and ionized atoms to form. As these ionized atoms transition to stable states, they emit characteristic X-rays that are specific to each element present in the sample. These emitted X-rays are detected by a specialized detector, which generates a spectrum representing the energy and intensity of the X-rays. By comparing the detected X-ray peaks to a calibration curve obtained from known reference standards, the concentrations of elements in the sample can be determined. The variations of the Cr_2O_3 content were studied under different experimental conditions. Throughout the experiment, various measurements were collected, including mass loss, heat treatment, crucible dissolution into the slag, wetting, and interaction of the slag with the substrate. All measurements were taken using standardized protocols and calibrated instruments to ensure accuracy and consistency. The analysis was conducted using XRD, SEM, EDS, H-T optical measurements, and FactSage for the thermodynamic study of the slag's behavior.

Chapter 4

RESULTS

4.1 Themodynamics of Slag

Crystallization and Phase Transformation of Slags

In this study, FactSage 8.2 was utilized to analyze the equilibrium phase and the mass fraction of precipitated solids in a slag system. The temperature range investigated spanned from 2000°C to 1000°C, with intervals of 100°C. The Equilib module in FactSage was employed, employing the FToxid database, which is based on the principle of minimizing Gibbs's free energy. The results, as depicted in the accompanying figure 4.1, indicate that the initial stage of slag precipitation is characterized by the formation of metal oxides. Interestingly, the quantity of metal oxide precipitation demonstrates minimal variations as the Cr_2O_3 content ranges from 1wt% to 3wt%, with fixed Al_2O_3 and MgO contents of 6wt% and 9wt%, respectively. Furthermore, the presence of a silicate phase, specifically Ca_2SiO_4, is observed in both slag compositions, denoted as S1 and S2 as shown in table 3.1. Notably, as the Cr_2O_3 content increases from 1wt% to 3wt%, spinel phase formation is enhanced, while maintaining a constant slag basicity of 2.4.

Figure 4.2 (a) illustrates the liquidus temperatures and complete solidification temperatures of the slag samples with varying Cr_2O_3 content. It is noteworthy that both the liquidus temperature (the temperature at which the first solid phase appears in the system) and the complete solidification temperature of the slags exhibit a decreasing trend in the slag increases from S1-1wt% Cr_2O_3 to S2-3wt% Cr_2O_3. Furthermore, the proportions of the slag liquid phase and solid phase were calculated

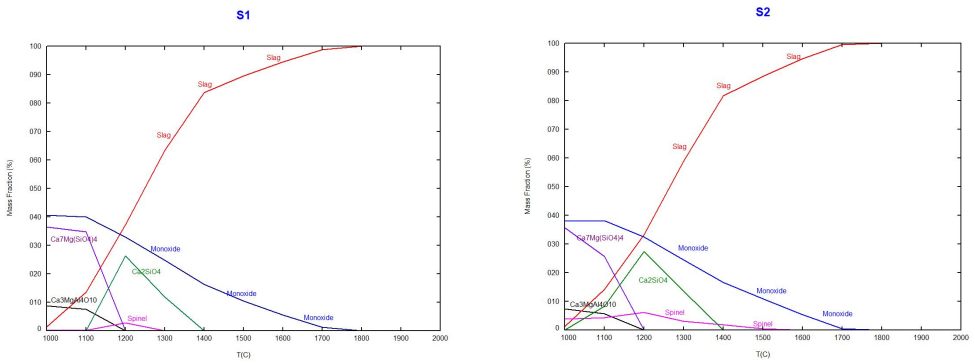

(a) (b)

Figure 4.1: Equilibrium Phase Compositions of the High-FeO Slags at Various Temperatures. (a) S1: Cr_2O_3 1wt% , (b) S2: Cr_2O_3 3wt%

using FactSage 8.2. As depicted in figure 4.2(b), the proportion of the slag liquid phase decreased, while the proportion of the solid phase increased with increasing Cr_2O_3 content, particularly up to 1500°C, primarily due to the formation of spinel compounds resulting from the high Cr_2O_3 content. However, the proportion of the solid phase decreased from 1400°C to 1600°C as the phases dissolved into the liquid at high temperatures. Following the pre-melting process, a substantial quantity of

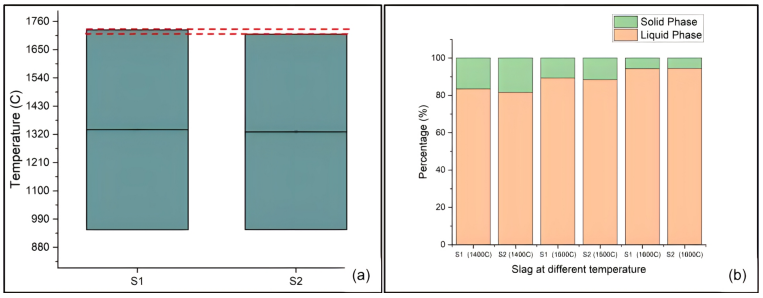

Figure 4.2: (a) Liquidus Temperatures and Complete Solidification Temperatures: S1 &S2, (b) Variation of the Liquid Phase and Solid Phase of the Slag with Different Cr_2O_3 Content I.E S1=1wt% and S2=3wt% at 1400, 1500, and 1600°C.

Al_2O_3 has been dissolved into the slag. To gain a comprehensive understanding of

the characteristics and behavior of the alumina-dissolved slag in response to temperature variations, it is imperative to analyze the phase fraction, as detailed in Table 3.2. The temperature range between 1000°C and 2000°C holds particular significance in comprehending the slag's properties. Utilizing FactSage 8.2, figure 4.3 provides a visual representation of the phases present within the slag during this temperature range. It is observed that the compositions S1-1wt% Cr_2O_3-Al_2O_3 and S2-3wt% Cr_2O_3-Al_2O_3 generate a substantial amount of the spinal phase in comparison to the original S1-1wt% Cr_2O_3 to S2-3wt% Cr_2O_3 slag compositions. Additionally, the mellite is present till 1400°C. S1-Al_2O_3 generates the TiSp phase (refers to the formation of a spinel structure involving titanium and other elements phase) which is not present in the S2-3wt% Cr_2O_3-Al_2O_3. Notably, the spinal phase is more prevalent in the S2-3wt% Cr_2O_3-Al_2O_3 composition than in the S1-1wt% Cr_2O_3-Al_2O_3 composition which depicts that due to high Cr-Content, the Cr has more affinity in the spinal phase than Ti. This finding corroborates the earlier argument that an increase in Cr_2O_3 content within the slag leads to its formation into the spinal phase. These scientific observations highlight the influence of temperature on the phase distribution within the alumina-dissolved slag and the impact of varying compositions such as Al_2O_3 and Cr_2O_3 on the formation of specific phases. In the context of the pre-melting process, a notable outcome is the substantial dissolution of Mo into the slag. This phenomenon prompts a comprehensive investigation into the characteristics and behavior of the Mo-dissolved slag, particularly with respect to temperature variations. A key aspect of this analysis involves studying the phase fraction, as outlined in Table 3.3. Notably, the temperature range between 1000°C and 2000°C holds significant importance in unraveling the slag's properties. By leveraging the powerful capabilities of FactSage 8.2, it becomes possible to visualize the phases present within the slag during this specific temperature range, as depicted in figure 4.4. The

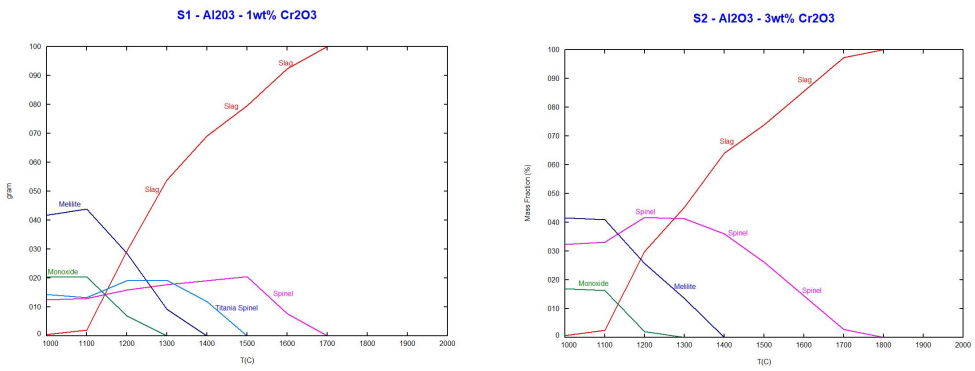

(a) (b)

Figure 4.3: Equilibrium Phase Compositions of the High-feo Slags at Various Temperatures. (a) S1-Al_2O_3: Cr_2O_3 1wt%, (b) S2-Al_2O_3: Cr_2O_3 3wt%

observations drawn from the analysis reveal intriguing insights into the behavior of the slag, particularly in relation to the compositions S1-Mo and S2-Mo. The generation of a substantial amount of the (CaO)(MoO_3) phase in both compositions, albeit to varying extents, showcases the influence of MoO_3 on the phase distribution. Additionally, the presence of Ca_2SiO_4 until 1350°C adds another layer of complexity to the system. Notably, the formation of the spinal phase in S1-Mo and S2-Mo, but the decreased Ca-Mo affinity in S1-Mo and more Mo going into the spinal with Cr in S2-Mo slag, highlights the role of composition, specifically the Cr_2O_3 content, in shaping the phase constituents. These scientific observations shed light on the intricate interplay between temperature, phase distribution, and the varying compositions of Mo and Cr_2O_3 within the slag. The significant elevation in the Al_2O_3 and MoO_3 content within the slag has resulted in a noticeable increase in the proportions of both the slag's liquid phase and solid phase when compared to the original S1-1wt% Cr_2O_3 to S2-3wt% slags.

The utilization of FactSage 8.2 has facilitated the calculation of the solid fraction in the slags, as depicted in figure 4.5 at 1500°C and 1600°C. The analysis reveals

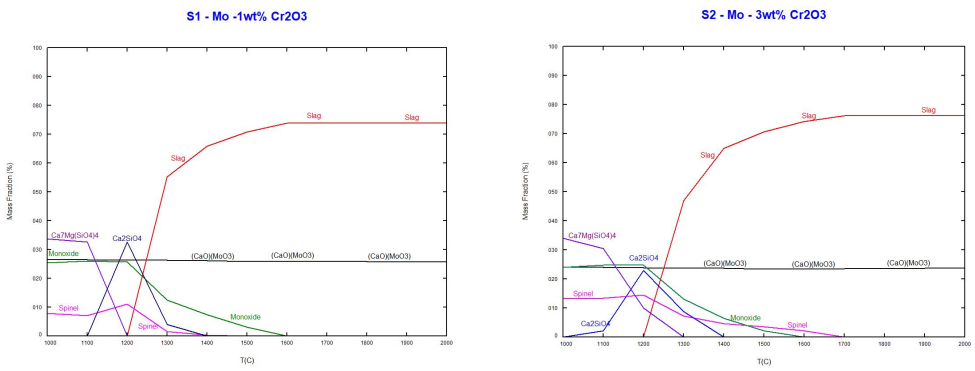

(a) (b)

Figure 4.4: Equilibrium Phase Compositions of the High-FeO Slags at Various Temperatures. (a) S1-Mo: Cr_2O_3 1wt% , (b) S2-Mo: Cr_2O_3 3wt%

a decrease in the proportion of the slag's liquid phase alongside an increase in the proportion of the solid phase with the progressive dissolution of Al_2O_3 and MoO_3 in the slag. Notably, the dissolution of MoO_3 demonstrates a more pronounced effect on the solid fraction content when compared to the dissolution of Al_2O_3. This observation highlights that the presence of MoO_3 contributes to a greater extent in generating a higher proportion of the solid phase within the slag, thus influencing its overall composition.

Theoretical Calculation of the Interaction Between Slag and Substrate

The differences in wettability and corrosion between the slag and the crucible were related not only to their respective properties but also to the interface interaction between them. The interaction between the slag and the substrate at 1600°C was calculated using the equilibrium module in FactSage 8.2. The system under investigation consists of two types of slag: S1 with 1 wt% Cr_2O_3 and S2 with 3 wt% Cr_2O_3. The composition of the slag was further modified by varying the content of different components, namely Al_2O_3, MoO_3, and MgO. The interaction between the slag and

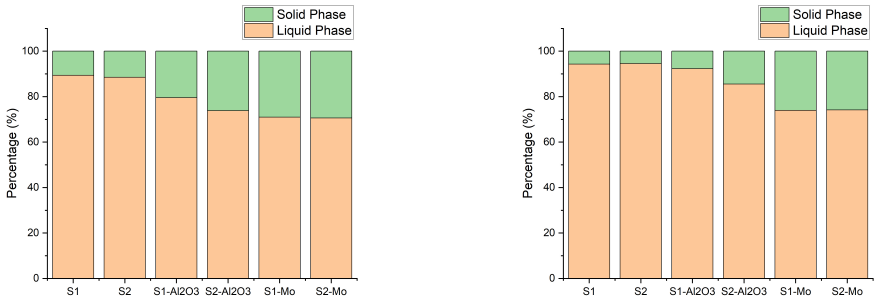

(a) (b)

Figure 4.5: Variation of the Main Phases i.e Liquid Phase and Solid Phase for the Slag: S1, S2, S1-Al_2O_3, S2-Al_2O_3, S1-Mo, and S2-Mo at (a)1500°C, (b)1600°C

the substrate was calculated at a high temperature of 1600°C using the equilibrium module. The results of these calculations are presented in figure 4.6 4.7 4.8, which likely shows a plot depicting the influence of changing Cr_2O_3 wt% in the slag on its interaction with the Crucible Al_2O_3, Mo and MgO. Based on the plots, it can be inferred that increasing the wt% of Cr_2O_3 in the slag enhances its affinity towards the spinal phase. The spinal phase refers to a crystalline structure that contains both divalent and trivalent metal ions, such as Cr^{2+} and Cr^{3+}. This increased affinity could be beneficial in terms of slag-crucible interactions, as it may lead to improved wettability.

Quantitative analysis

The mass loss study aimed to investigate the behavior of the slags and Mo crucible before and after the pre-melting experiment. Table 4.1 presents the measured mass loss data for the slag S1-1wt% Cr_2O_3 to S2-3wt% Cr_2O_3 slags and Mo crucible samples before and after the experiment. The results indicate a gradual decrease in the mass of the Mo crucible after each pre-melting run, while there is an increase in

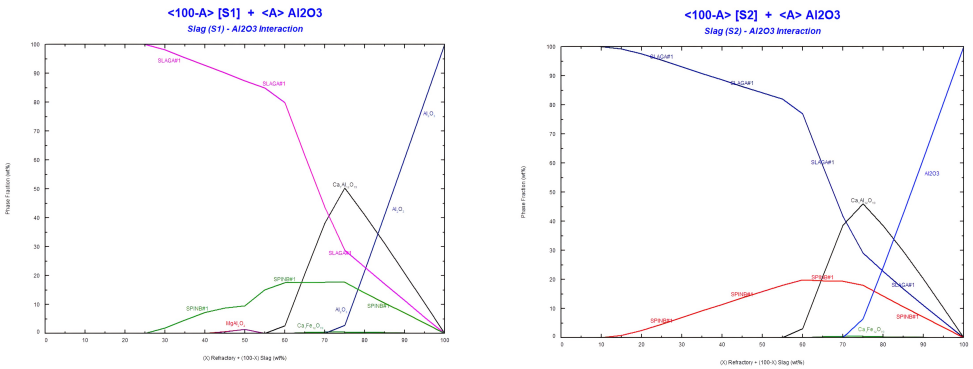

(a) a (b) b

Figure 4.6: Interaction Between Slag (a)S1-1wt% Cr_2O_3, (b) S2-3wt% Cr_2O_3 and Al_2O_3 Substrate.

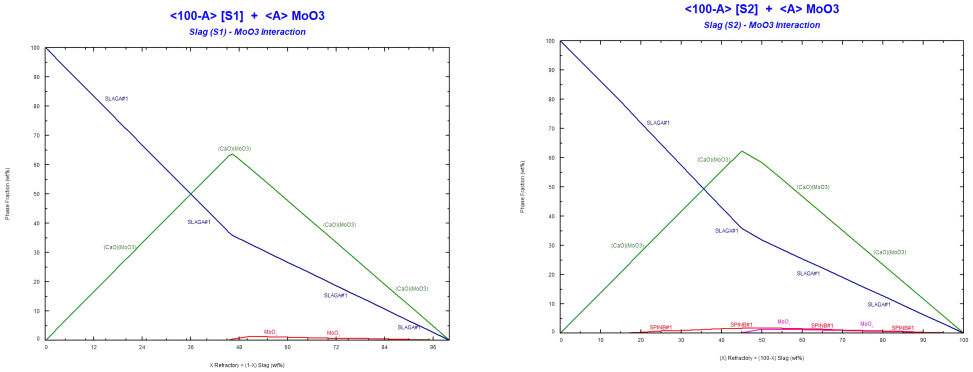

(a) a (b) b

Figure 4.7: Interaction Between Slag (a)S1-1wt% Cr_2O_3, (b) S2-3wt% Cr_2O_3 and Mo Substrate.

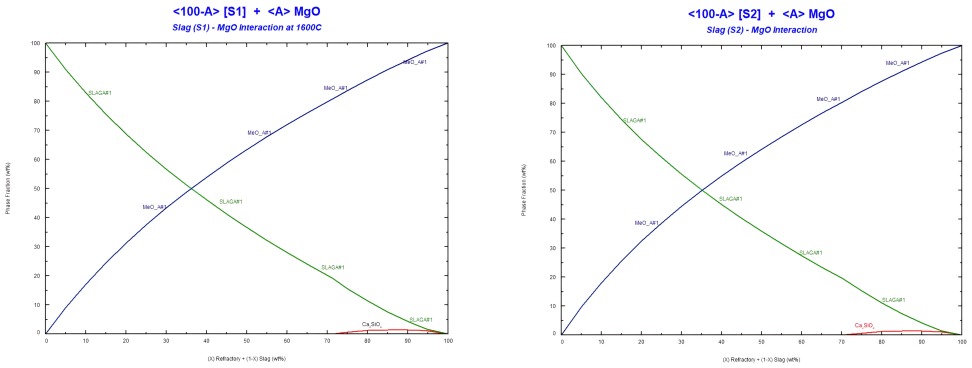

(a) a (b) b

Figure 4.8: Interaction Between Slag (a)S1-1wt% Cr_2O_3, (b) S2-3wt% Cr_2O_3 and MgO Substrate.

the mass of the slag.

The observed mass loss can be attributed to various factors, including evaporation, volatilization, and chemical reactions occurring within the slag and crucible materials. It is important to note that the reported mass loss values represent the cumulative effect of these processes over the duration of the experiment. Consequently, the significant degradation of the crucible after each run reflects the reaction between the slag and the crucible as shown in figure 4.9. Furthermore, it is noteworthy that the Mo crucible used for the S2-3wt% Cr_2O_3 slag composition is more affected than in the S1-1wt% Cr_2O_3 composition, likely due to the higher Cr_2O_3 content in the S2 slag. The gradual decrease in the mass of the crucible suggests enhanced material degradation and vaporization at higher temperatures. This can be attributed to the higher thermal energy available, leading to increased diffusion and reaction rates within the slag and crucible. It is worth noting that the mass gain of the slag indicates the dissolution of the slag composition with the Mo content. This information is valuable for understanding the behavior of the slag during the pre-melting process and its potential impact on the overall system. Overall, the mass loss study

Experiment		Mo Crucible	Slag	Mass Loss (wt%)	Mass Gain (wt%)
Mass Loss - S1-Mo Composition					
Run 1	Before	67.15	17.70	1.33	4.34
	After	66.26	18.47		
Run 2	Before	66.15	15.78	1.42	2.85
	After	65.21	16.32		
Run 3	Before	65.12	15.30	1.56	1.96
	After	64.10	15.60		
Run 4	Before	64.08	15.75	1.68	0.38
	After	63.00	15.81		
Mass Loss - S2-Mo Composition					
Run 1	Before	66.97	16.10	1.56	5.21
	After	65.92	16.94		
Run 2	Before	65.85	15.87	1.74	6.30
	After	64.70	16.87		
Run 3	Before	64.67	15.70	1.63	4.58
	After	63.61	16.42		
Run 4	Before	63.35	15.28	1.19	0.91
	After	62.59	15.42		

Table 4.1: Mass Loss: S1-Mo and S2-Mo Compositions

provides insights into the thermochemical behavior of the slag and crucible, shedding light on the effects of the crucible on slag contamination and volatilization. These findings contribute to a comprehensive understanding of the pre-melting process and can inform future studies on optimizing process parameters and material selection.

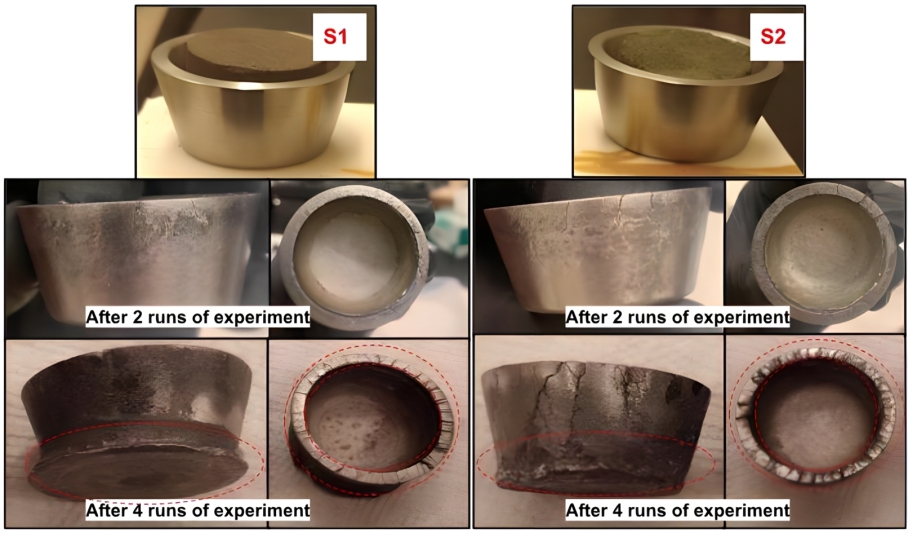

Figure 4.9: Degradation of Mo Crucible

Energy-dispersive X-ray spectroscopy [EDS]

The energy-dispersive X-ray spectroscopy (EDS) analysis of the slag provides valuable insights into its elemental composition. Through EDS analysis, it has been confirmed that molybdenum (Mo) is present in the slag, along with other elements that are also detected as shown in figure 4.10. Based on the EDS, the MoO_3 is quantified as 12 to 14 wt%.

X–ray diffraction patterns

To determine the phases present in the slag samples, X-ray diffraction (XRD) analysis was conducted. Figure 4.11 displays the results of this analysis for the considered

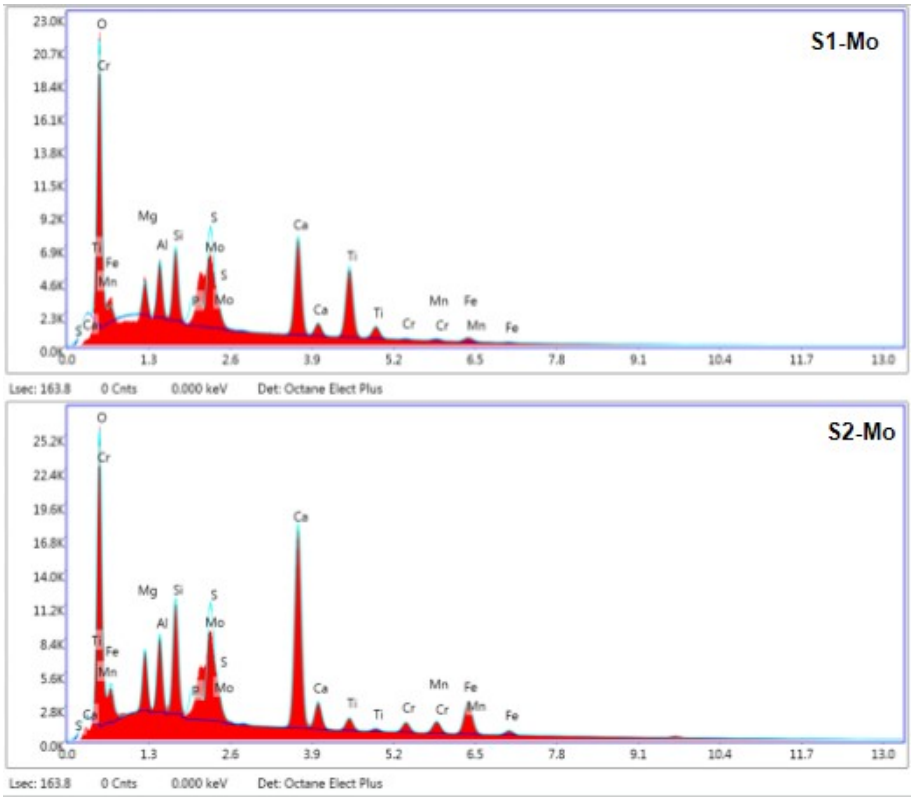

Figure 4.10: EDS Analysis of the S1-Mo and S2-Mo Powder

slag samples, namely S1-Mo and S2-Mo, aiming to investigate the phase formation of molybdenum (Mo) following the pre-melting process. The qualitative outcomes of X-ray diffraction revealed the presence of various phases in the samples. The dominant phases identified in both slag samples include Calcium Molybdate ($CaMoO_4$), Calcium Silicate (Ca_2SiO_4), Calcium Chromium Molybdenum Oxide (CaCrMoO), and Iron Oxide (FeO). The detection of Calcium Molybdate in the diffraction patterns further supports the formation of crystalline solids within the slag after employing a Mo crucible during pre-melting. In figure 4.11, it can be observed that in sample S2-Mo, in addition to the phases reported in sample S1-Mo, there is a higher occurrence of Calcium Chromium Molybdenum Oxide. This finding aligns with the higher chromium content observed in the slag, thereby justifying the increased presence of

Calcium Chromium Molybdenum Oxide in S2-Mo. These scientific observations obtained from XRD analysis provide valuable insights into the phase composition of the slag samples, shedding light on the formation of specific crystalline phases, especially Calcium Molybdate, and the influence of varying compositions on the phase distribution within the slag.

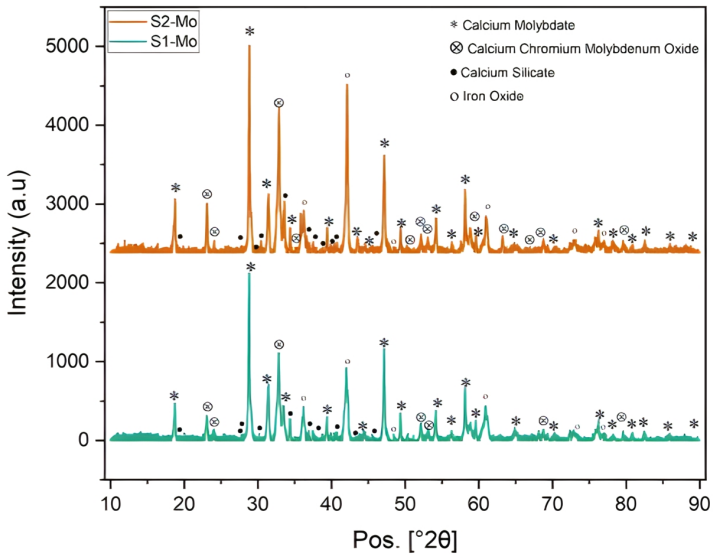

Figure 4.11: Identified Phases by the XRD Technique for Slags S1-Mo and S2-Mo

4.2 H-T Optical Image Surface Tension Measurement

The melting process of each slag sample and the morphological change of slag droplets at different temperatures is recorded by the High-temperature optical CCD camera. The slag melting and the change of droplet morphology of S1-1wt% Cr_2O_3-Mo and S2-3wt% Cr_2O_3-Mo are shown in figure 4.12. It can be seen from the pictures that the spreading processes of different slag pellets on the MgO substrate were about the same, although the melting temperatures were not. With the slag droplet spreading on the substrate, the height of the slag gradually decreased, and so did

the contact angle. In figure4.12 (a), it is evident that the slag S1-Mo initiates its melting at a significantly higher temperature compared to the S2-Mo slag as shown in 4.12 (b). Even after reaching a temperature of 1650°C, the S1-Mo slag exhibits greater retention of slag on the substrate, whereas the S2-Mo slag forms a flatter pool. This difference in behavior can be attributed to the presence of the (CaO)(MoO_3) phase, which is abundant in both slags even at higher temperatures. Additionally, the slag S2-Mo contains a higher concentration of Cr_2O_3. As a result, some of the molybdenum (Mo) present in the S2-Mo slag forms a spinal phase, which has a lower melting point. Consequently, there is a lower retention of the slag on the surface of the S2-Mo slag compared to the S1-Mo slag. The formation of the (CaO)(MoO_3) phase and the influence of Cr_2O_3 on the melting behavior of the slags contribute to the observed differences in their melting morphology.

In studying the interaction between slags and solid surfaces, the utilization of different substrates serves multiple important purposes. One crucial objective is to assess material compatibility, as other materials can exhibit varying reactions and structural changes when exposed to specific molten materials at high temperatures. Another significant aspect investigated through the use of different substrates is wettability. The present study also examines the wetting and interaction behavior of slag S2-Mo on three distinct substrates: MgO block, MgO single crystal, and Mo. The use of a MgO single crystal (refer figure 4.15) substrate in addition to the employed MgO block enables the investigation of the differences in the ability of molten slag to spread and adhere to solid surfaces. The observed variations in wetting behavior are attributed to the differences in porosity, surface energies, and roughness between the two substrates. Utilizing the MgO block leads to noticeable infiltration of the slag, whereas penetration into the substrate is minimal when employing the single crystal. Furthermore, the morphology of the molten slag appears to be more uniform on the

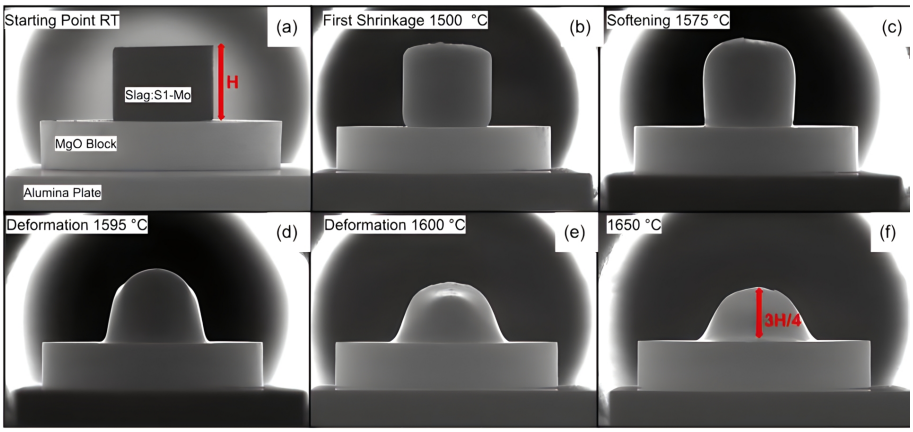

(a) a

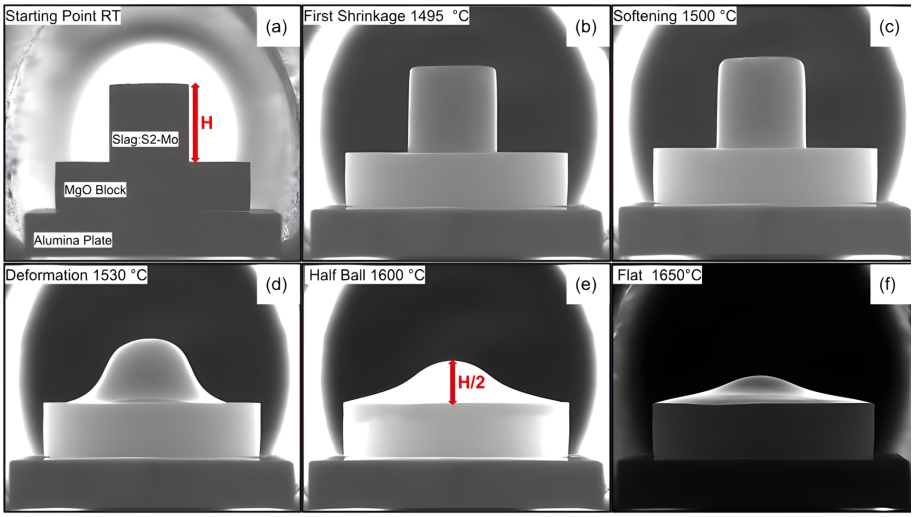

(b) b

Figure 4.12: Melting Characteristic Temperature of Slag Composition (a) S1-Mo, (b) S2-Mo on MgO Block Substrate

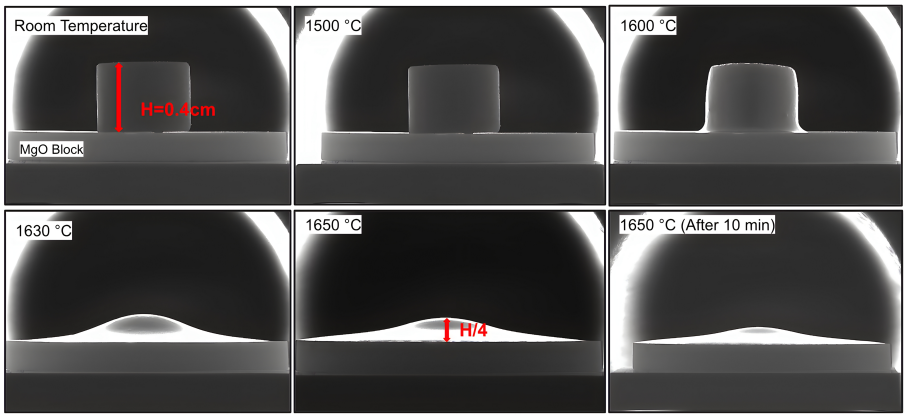

(a) a

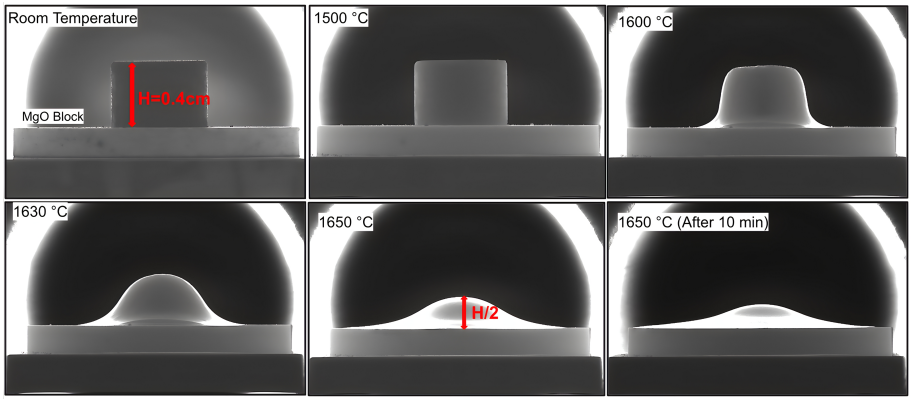

(b) b

Figure 4.13: Melting Characteristic Temperature of Slag Composition (a) S1-MgO, (b) S2-MgO on MgO Block Substrate

single crystal substrate than on the block. Furthermore, the choice of Mo substrate allows for the examination of adhesion and retention properties. Different substrates can possess varying adhesion forces, affecting the extent to which the droplets adhere to and are retained on the surface. By using Mo substrates, it has been observed that there is no such adherence of the slag on the surface of Mo (see figure 4.15), unlike the MgO substrates. The slag tends to run off from the Mo substrate at high temperatures.

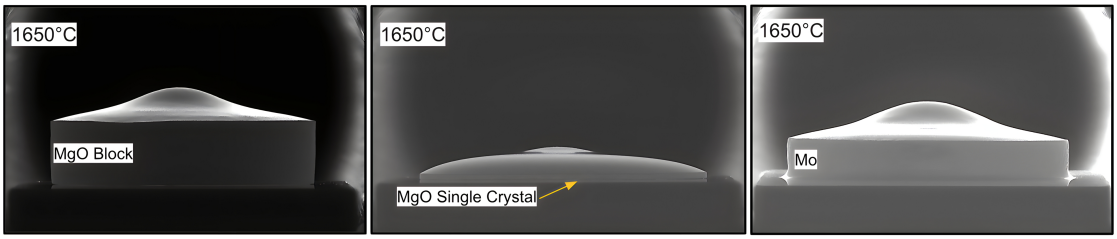

Figure 4.14: Melting Characteristic Temperature of Slag Composition MgO Block, MgO Single Crystal, and Mo Substrates

Surface Tension

Surface tension, a crucial parameter characterizing surface properties, exhibits a direct correlation with the wetting phenomenon. The wetting ability of a liquid improves as its surface tension decreases. The measurement of surface tension entails examining its dependence on temperature and the chemical composition of the slag. To present the surface tension variation with temperature, a calculation method was employed, as discussed in the relevant section and illustrated in the accompanying figure. The values below 1600°C were omitted due to the presence of solid particles within the pellet. The figures demonstrate the relationship between the surface tension of the chosen molten slag and temperature. It is observed that the surface tension of the slag decreases linearly with increasing temperature. This behavior can be attributed to the heightened thermal movement of ions within the slag as the temperature rises. Consequently, the inter-particle spacing increases, resulting in a weakened interaction force between the liquid particles and the particles residing on the liquid surface. Consequently, the surface tension of the molten slag decreases. Based on the obtained results, as depicted in the figure, it is apparent that the surface tension of slag S2-Mo is lower than that of slag S1-Mo across all temperatures. This difference arises due to the elevated presence of Cr_2O_3 in the S2-Mo slag. The

affinity between Mo and Cr_2O_3 enhances the wettability of the slag, thereby reducing its surface tension.

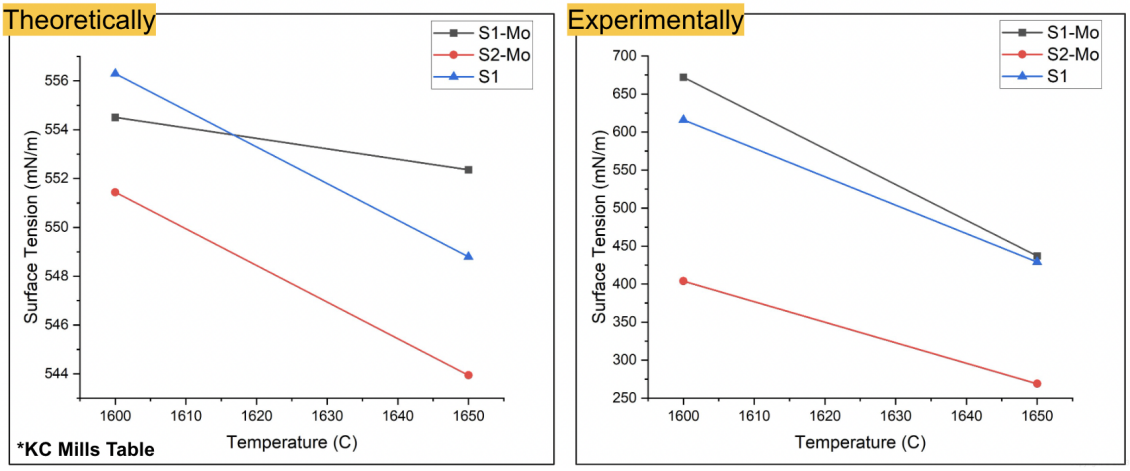

Figure 4.15: Dependence of Surface Tension Versus Temperature.

4.3 Foaming Index

The Slag Foaming Index provides valuable insights into the ability of slags to generate and maintain stable foam in steelmaking. In this study, we investigated the index of different slag compositions to assess their foam stability characteristics. The findings indicate a significant variation in the index values among the tested slag compositions. In this study, the foaming index of Electric Arc Furnace (EAF) slags with varying Cr_2O_3 content was investigated. The chemical compositions of three slag samples, slag S1-Mo contained 1.24 wt% Cr_2O_3 and 19.09 wt% MoO_3, while Slag S2-Mo consisted of 3.39 wt% Cr_2O_3 and 17.27 wt% MoO_3. The original industrial Slag S1 contained 1.07 wt% Cr_2O_3. To ensure accurate calculations, MoO_3 and P_2O_5 were excluded from the slag compositions, and the compositions were recalibrated to 100% as shown in table 4.2. The KC Mills - Iida Model was employed to calculate the liquid viscosity of the slag at a temperature of 1600°C. The solid fraction of the

slag was determined using FactSage 8.2 software. The Effective viscosity of the slag was determined using the Einstein-Roscoe equation, which takes into account the amount and size distribution of solid particles present. The Einstein-Roscoe equation provides insights into how the presence of solid phases and their size distributions affect the effective viscosity of the slag. It plays a crucial role in understanding the flow behavior of the slag and its foamability characteristics. The obtained results for the Cr_2O_3 varying EAF slags given in the table 4.3, include the Cr_2O_3 content (wt%), liquid viscosity at 1600°C (poise), solid fraction at 1600°C, effective viscosity at 1600°C (poise), surface tension (N/m), and density (kg/m^3). The foaming index equation 2.10, represented by the symbol $\sum$, was determined for each slag composition using the data from table 4.3. The foaming index for the S1 slag was measured as 14.13 seconds, while the S1-Mo slag exhibited a slightly higher foaming index of 16.13 seconds. The S2-Mo slag demonstrated the highest foaming index among the tested compositions, with a value of 19.38 seconds, as the trend shown in figure 4.16. It should be noted that a constant value of 999 for a MgO-saturated slag was used for the calculation of the foaming index. Additionally, the density of the slag was assumed to be 2700 kg/m^3 for all the compositions. These results provide valuable insights into the viscosity, solid fraction, effective viscosity, surface tension, density, and foaming index of the Cr_2O_3 varying EAF slags. Understanding these parameters is essential for evaluating the foam stability and potential applications of these slags in various industrial processes.

Sample	Al_2O_3	CaO	Cr_2O_3	FeO	MgO	MnO	SiO_2	TiO_2
S1	6.18	32.82	1.07	29.81	9.68	5.97	13.83	0.61
S1-Mo	8.06	37.62	1.24	23.49	7.34	6.51	15.17	0.61
S2-Mo	7.97	35.31	4.11	23.42	7.33	6.28	14.98	0.57

Table 4.2: Composition of the Slags by Excluding MoO_3 Effect

Sample	wt%	Liq. Viscosity (poise)	Solid Fraction	Eff. Viscosity (poise)	Surface Tension (N/m)	Density (kg/m^3)
S1	1.07	0.498596	0.0568	0.577	0.616	2700
S1-Mo	1.24	0.650785	0.0222	0.688	0.672	2700
S2-Mo	4.11	0.625158	0.0098	0.641	0.404	2700

Table 4.3: Properties of the Slag at 1600°C

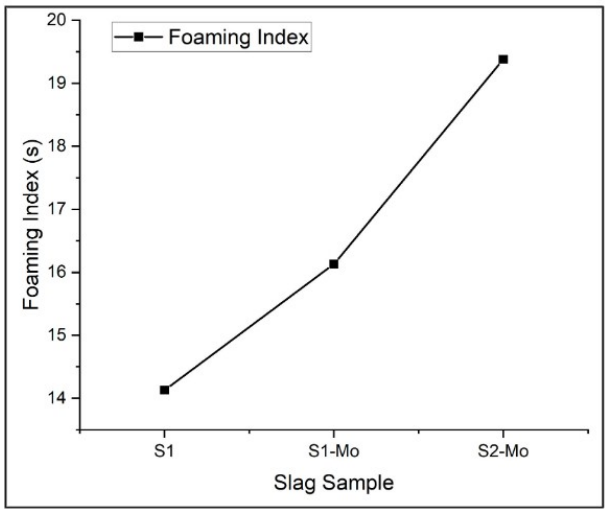

Figure 4.16: Foaming Index Result for Various Slag Systems at 1600°C

Chapter 5

DISCUSSIONS

The study of slag metallurgy and the influence of surface-active oxides present a dynamic and critical aspect that requires careful management and understanding. Surface-active oxides play a significant role in shaping the properties and behavior of slag, particularly regarding surface tension. High FeO content in slag has been identified to induce corrosive behavior and lead to crucible dissolution, highlighting the importance of maintaining appropriate FeO levels. The addition of Cr2O3 has been found to promote spinel formation in high-temperature slag, impacting slag composition and performance. Notably, research indicates that a higher content of Cr2O3 results in lower surface tension of the slag across various temperatures. Furthermore, the presence of Calcium Chromium Molybdenum Oxide in Cr2O3-Mo slag improves wetting behavior, while spinel phase formation is observed in both slag compositions, with greater Mo incorporation in the 3 wt% Cr2O3 variant. Increasing Cr2O3 content enhances the foaming effect of slag. Accurate measurement of surface tension in low capillary constant melts can be achieved through the constrained drop method. Wetting behavior on a substrate is influenced by factors such as surface energy, intermolecular forces, and surface roughness. By discussing these aspects in the thesis, a comprehensive understanding of the interplay between surface-active oxides and slag behavior can be attained, offering valuable insights for optimizing slag metallurgy processes.

Chapter 6

FUTURE WORK

The study has provided valuable insights into the thermophysical properties of EAF slag containing Cr_2O_3. The following research directions can contribute to a more comprehensive understanding:

- To gain a comprehensive understanding, the studies will be expanded to cover a wider range of slag compositions. By investigating a broader composition range, the effects of surface-active oxides, including Cr_2O_3, can be thoroughly examined, providing insights into their role in slag metallurgy.
- To establish reliable correlations, synthetic slag compositions will be developed, precisely matching specific chemical compositions. This correlation will serve as a solid foundation for studying the influence of surface-active oxides on slag properties and behavior, facilitating more accurate and targeted analyses.
- A vital aspect of this research will involve measuring the viscosity of slag samples to understand the impact of Cr_2O_3 and other surface-active oxides. The optimization of slag flow and control during industrial processes can be achieved by comprehending their effects on slag viscosity.
- An essential aspect of slag metallurgy is selecting appropriate crucibles to minimize dissolution and maintain consistent slag composition. The research will focus on optimizing crucible selection by exploring different materials and designs that can withstand slag's corrosive nature, ensuring the crucible's integrity.
- To enhance accuracy and relevance, the sessile drop experiment will be improved by employing substrates that closely resemble industrial conditions. By utilizing substrates with similar surface properties and compositions, the wet-

ting behavior of slag can be studied under conditions that closely simulate real-world scenarios.

- The research will utilize confocal high-temperature scanning microscopy to investigate slag behavior and structural changes in real time at elevated temperatures. This advanced technique will enable the observation of phase transformations and other phenomena during slag processing, providing valuable insights into the dynamic nature of slag.
- Raman spectroscopy will be employed to characterize the molecular structure, phase composition, and properties of slag materials. This analytical technique will contribute to a deeper understanding of slag behavior, enabling the correlation of molecular structure with performance and facilitating informed process optimization.

REFERENCES

[1] worldsteel.org. https://worldsteel.org.

[2] Calvimontes. A thermodynamic approach to predict apparent contact angles on microstructures using surface polygonal maps. *Soft Matter*, 1(41):838–8323, 2014.

[3] Tunc Camdali, M., and G. Arasil. Analysis of an electric arc furnace used for casting of steel: An exergy approach. *Metallurgist (New York)*, 64(5-6):483–495, 2020.

[4] F. Cooper and J. A. Kitcher. Jisi. *JISI*, 193:48–55, 1959.

[5] Lotte De Vos, Tim Van Gucht, Bart Blanpain, Guido Vanermen, and Patrick Wollants. Critical assessment of the applicability of the foaming index to the industrial basic oxygen steelmaking process. *Steel Research International*, 92(1):2000282, 2021.

[6] S. Hara, M. Ikuta, M. Kitamura, and M. Ogino. Tetsu-to-hagane. *Tetsu-to-Hagane*, 69:1152–1159, 1983.

[7] K. Ito and R.J. Fruehan. Metallurgical transactions b. *Metallurgical Transactions B*, 20(4):509, 1989.

[8] K. Ito and R.J. Fruehan. Study on the foaming of cao-sio2-feo slags, part i: Foaming parameters and experimental results. *Metallurgical and Materials Transactions B*, 20:509–514, 1989.

[9] R. Jiang and R. J. Fruehan. ibid. *ibid*, 22B:481–489, 1991.

[10] S. Jung and R. J. Fruehan. Isij int. *ISIJ Int.*, 40:348–355, 2000.

[11] H.S. Kim, D.J. Min, and J.H. Park. Foaming behavior of CaO–SiO2–FeO–MgOsatd–X (x=al2o3, mno, p2o5, and caf2) slags at high temperatures. *ISIJ International*, 41(4):317–324, 2001.

[12] W.E. Lee and S. Zhang. Melt corrosion of oxide and oxide–carbon refractories. *International Materials Reviews*, 44(3):77–104, 1999.

[13] Q. Li, J. Gao, Y. Zhang, Z. An, and Z. Guo. Viscosity measurement and structure analysis of cr2o3-bearing cao-sio2-mgo-al2o3 slags. *Metall. Mater. Trans. B*, 48:346–356, 2016.

[14] Z. Liu, R. Dekkers, B. Blanpain, and M. Guo. Experimental study on the viscosity of stainless steelmaking slags. *ISIJ Int.*, 59:404–411, 2019.

[15] Matteo Sporchia. ELECTRIC ARC FURNACE AC (PART 2) The Raw Materials. https://www.linkedin.com/pulse/electric-arc-furnace-ac-part-2-raw-materials-matteo-sporchia/.

[16] N. Menad, Kana, A. Seron, and N. Kanari. New eaf slag characterization methodology for strategic metal recovery. *Materials*, 14(6):1513–, 2021.

[17] E.B. Pretorius and R.C. Carlisle. Foamy slag fundamentals and their practical application to electric furnace steelmaking. In *Proceedings of the 16th Process Technology Conference*, New Orleans, LA, USA, November 1998.

[18] G. Qiu, L. Chen, J. Zhu, X. Lv, and C. Bai. Effect of cr2o3 addition on viscosity and structure of ti-bearing blast furnace slag. *ISIJ Int.*, 55:1367–1376, 2015.

[19] R. E. Roth, R. Jiang, and R. J. Fruehan. Trans. iss. *Trans. ISS*, 19:55–63, 1992.

[20] Seetharaman, A. McLean, R. Guthrie, and S. Sridhar. *Treatise on Process Metallurgy: Volume 1, Process Fundamentals*. Elsevier, 2014.

[21] SubsTech. Materials engineering. `http://www.substech.com/`.

[22] J. H. Swisher and C. L. McCabe. Trans tms-aime. *Trans TMS-AIME*, 230:1669–1675, 1964.

[23] J. Terrones-Saeta, Suárez-Macías, E. R. Moreno-López, and F. A. Corpas-Iglesias. Determination of the chemical, physical and mechanical characteristics of electric arc furnace slags and environmental evaluation of the process for their utilization as an aggregate in bituminous mixtures. *Materials*, 14(4):1–16, 2021.

[24] Union Carbide Corporation. *UCAR Electric Arc Furnace Electrode Digest*. Union Carbide Corporation, Carbon Products Division, Chicago, 1975–1980.

[25] C. Xu, W. Wang, L. Zhou, S. Xie, and C. Zhang. The effects of cr2o3 on the melting, viscosity, heat transfer, and crystallization behaviors of mold flux used for the casting of cr-bearing alloy steels. *Metall. Mater. Trans. B*, 46:882–892, 2014.

[26] R.Z. Xu, J.L. Zhang, Z.Y. Wang, and K.X. Jiao. Influence of cr2o3 and b2o3 on viscosity and structure of high alumina slag. *Steel Res. Int.*, 88:1600241, 2017.

[27] Y. Zhang and R. J. Fruehan. Metall, and mater. trans . *Metall, and Mater. Trans* , 26B:803–812, 1995.